UNIVERSITY OF CALIFORNIA, MERCED

PEDOT Nanowires for Energy Storage: Synthesis and Property

A thesis submitted in partial satisfaction of the requirements
for the degree of

MASTER OF SCIENCE

In

CHEMISTRY AND CHEMICAL BIOLOGY

By

WU YING

Committee in charge:

Professor Anne Myers Kelley, Chair
Professor Erik Menke, Advisor
Professor Tao Ye
Professor Vincent C. Tung

2014

This page is reserved for copyright statements.

The thesis of Wu Ying is approved, and it is acceptable in quality and form for publication on microfilm and in digital formats:

Professor Tao Ye

Professor Vincent C. Tung

Professor Erik Menke, Advisor

Professor Anne Myers Kelley, Chair

University of California, Merced

2014

DEDICATION

To my parents, brother, and whom I miss

Table of Contents

List of Figures

Page

List of Tables

Page

Acknowledgements

I am thankful for the support from my family and friends, without whom I could not have completed this work.

I would like to give my special thanks to my graduate research adviser, Dr. Erik Menke, for his patience and guidance in my growth as a scientist and engineer. I would also like to extend my gratitude to my dissertation committee: Dr. Anne Kelley, Dr. Tao Ye and Dr. Vincent Tung. Additionally, I was extraordinarily lucky to have had the opportunity to work with the brilliant graduate student, Luke Reed; I thank him for his helpful suggestions and wish him the best in his career. I also would like to thank many other talented graduate students and undergraduates with whom I have worked.

I am also grateful to the scientific mentors I have had as an undergraduate, in particular Dr. Yi Xie and Yujie Xiong at University of Science and Technology of China, for providing my first opportunities to develop as a researcher.

I also want to thank Gary Abel for his kind help with the AFM experiments.

I would also like to thank the University of California, Merced for the financial support and the graduate school council project at the university.

Resume

EDUCATION

M.S., Physical Chemistry, **University of California, Merced** 2012~2014

B.S., Chemistry, **University of Science and Technology of China** 2008~2012

RESEARCH EXPERIENCE

Research Assistant at University of California, Merced

Project: PEDOT Nanowires and Carbon Materials for Energy Storage

Synthesized PEDOT nanowire by lithographically patterned nanowire electrodeposition (LPNE) and characterized PEDOT using AFM, SEM and Raman Spectroscopy;

Tested the electrochemical performance of PEDOT nanowires as cathode material in $AlCl_3$:EMIC as the electrolyte

Synthesized Ni nano catalyst via polymer template and grew CNF via plasma enhanced chemical vapor deposition (PECVD);

Prepared carbon-based battery electrodes by electrodepositing functional nano-clusters on CNF and tested the thermal stability of the functional nano-clusters and the performance of the battery electrodes

Undergraduate Research Assistant at University of Science and Technology of China

Project: Energy Saving Materials for Smart Windows

Synthesized tungsten doped VO_2 via hydrothermal method to lower the metal–insulator transition temperature;

Analyzed the crystal structure of tungsten doped VO_2 via XRD and utilized infrared spectroscopy to identify structural changes in doped VO_2.

EXPERIMENTAL SKILLS

Raman Spectroscopy, AFM, XRD, UV-Vis spectrometry, Infrared Spectroscopy;

Physical Vapor Deposition (PVD), Chemical Vapor Deposition (CVD), PECVD, Potential Stat, Photolithography, Glovebox, Clean Room Techniques

PUBLICATIONS AND PRESENTATIONS

Recent Progress on PEDOT based Supercapacitors, Submitted to J. Electrochem. Soc.

The Relationship between Synthesis and Performance for PEDOT Nanowires, Poster for 2014 Material Research Society Spring Meeting

Effective Communication in Science and Engineering, Talk in 2014 You See Leadership Conference

High Power Nickel-Iron Battery Using Hybrid Nanowires, Poster for Chemistry Seminar in UC Merced

Identifying Structural Distortion in Doping VO_2 with IR Spectroscopy, Phys. Chem. Chem. Phys. 14, 7225-7228

PROFESSIONAL AFFILIATION

Material Research Society

COMPUTER AND DATA SKILLS

COMSOL Multiphysics, Microsoft Office, Matlab, Python

SCHOLARSHIP AND HONOR

Graduate Student Travel Fellowship	UC Merced	2014
Graduate Research Council Fellowship	UC Merced	2014
Summer Research Fellowship	UC Merced	2013

Abstract of the Thesis

PEDOT Nanowires for Energy Storage: Synthesis and Property

By

Wu Ying

Master of Science in Chemistry and Chemical Biology

University of California, Merced, 2014

Professor Erik Menke, Advisor

PEDOT nanowires of different size and morphology were successfully synthesized in aqueous solution via lithographically patterned nanowire electrodeposition (LPNE) in order to establish a direct relationship between the synthesis conditions and the properties. Optical microscopy, atomic force microscopy (AFM), cyclic voltammetry and electrochemical impedance spectroscopy (EIS) are utilized to characterize the size, morphology and electrochemical properties of the resulting PEDOT nanowires. Optical microscopy and AFM show that the various electrodeposition parameters (deposition methods, deposition voltage, deposition time, template size, etc.) have a great impact on the materials properties of the prepared nanowires. EIS measurement demonstrates that those nanowires exhibit exceptional capacitive property compared to that of commercial capacitors and polymer dispersion capacitors.

1. Introduction

1.1 Conducting Polymer

Conductive polymers, also known as intrinsically conducting polymers, are polymers that conduct electricity. [1~4] It is generally recognized that the modern study of electric conduction in conjugated polymers began in 1977 with the publication by the group of MacDiarmid and Heeger at the University of Pennsylvania describing the doping of polyacetylene. [5] Since then, broad research on various kinds of conducting polymers continues. [1] [2] [5] Conducting polymers may have metallic conductivity or can be semiconductors as is shown in figure 1.

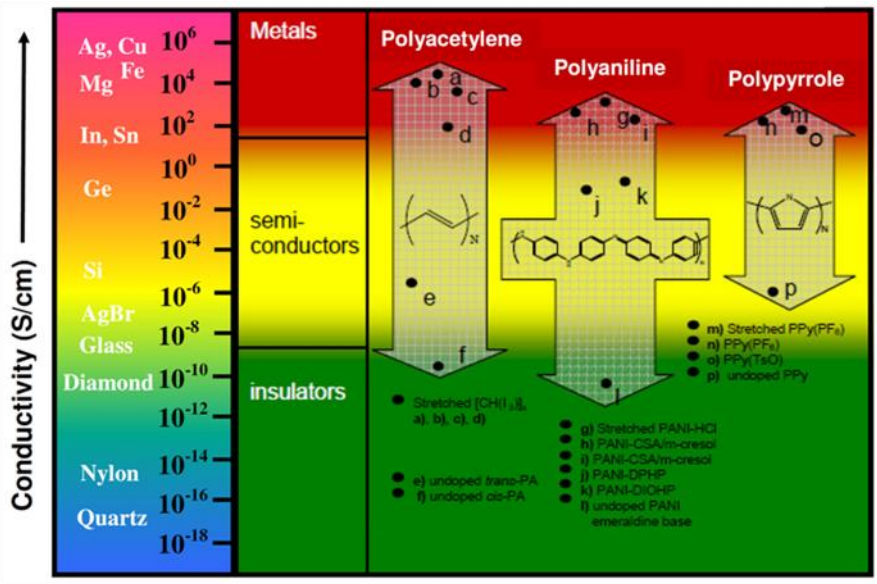

Figure 1. Conductivity of some conjugated polymers in comparison to typical metals, semiconductors or insulators. Reference [63]

In general, conjugated polymers have an overlap of pi-molecular orbitals to allow the formation of delocalized electron wave functions along the molecular backbone. The linear backbone "polymer blacks" (polyacetylene, polypyrrole, polythiophene and polyaniline) and their copolymers are the main class of conductive polymers. [1] [2] [5] Conducting polymers constitute an interesting class of materials as they combine some of the mechanical features of plastics with the electrical properties typical of metals. For this reason, they are often referred to as synthetic metals. [2] Conducting polymers are widely studied for potential applications such as batteries, photovoltaic, light-emitting diodes (OLEDs), electro chromic devices and electromechanical devices due to their relatively high conductivity and chemical stability. [3~13] The electrical properties of conducting polymers can be fine-tuned using the methods of organic synthesis and by advanced dispersion techniques. [14] [15] [16] Table 1 presents different types of conductive polymers according to their composition.

In terms of applications in electronics, especially in flexible electronics, conductivity, flexibility and transparency are the three most important characteristics that we care about. [17] Among those intensively investigated conducting polymers, such as poly(acetylene) (PAC), poly(pyrrole) (PPY), poly(aniline) (PANI) and poly(thiophene) (PT), PAC has the highest reported conductivity (up to 10^6 S/cm) while PANI can only achieve about 4.60×10^{-3} S/cm. [1] However, PAC is insoluble in water which limits its large scale application in industry. Further, as doped PPY films are usually dark colored either blue or black, PPY cannot be a good candidate for the electronic industry nowadays. [1] PEDOT

has the combined characteristics, for example, relatively high conductivity, transparency and potentially soluble in aqueous solution, which make it an ideal candidate for electronic applications. [1] [18]

Table 1. Types of conductive polymers according to their composition

The main chain contains	**Heteroatoms present**		
	No heteroatom	Nitrogen containing	Sulfur containing
Aromatic cycles	Poly(fluorene) polyphenylene polypyrene polyazulene polynaphthalene	poly(pyrrole) polycarbazole polyindoles polyazepines polyaniline	poly(thiophene) poly(3,4-ethylenedioxythiophene) poly(p-phenylene sulfide)
Double bonds	Poly(acetylene)		
Aromatic cycles and double bonds	Poly(p-phenylene vinylene)		

Table 2. Properties of four main types of conducting polymers

Conducting Polymers	**Conductivity (S/cm)**	**Transparency**	**Solubility in water**
PAC	10^5	No (Blue)	insoluble
PPY	100	No (Blue/Black)	insoluble
PANI	10^{-2}	Clear/colorless	soluble
PEDOT	1000	Nearly transparent	soluble (PEDOT:PSS)

1.2 Poly(3,4-ethylenedioxythiophene)

This new polythiophene derivative, poly(3,4-ethylenedioxythiophene) (PEDOT) was developed in the second half of the 1980s by the scientists at the Bayer AG research laboratories in Germany. [1] [5] The monomer of PEDOT is 3, 4-ethylenedioxythiophene (EDOT). As we can see in figure 2, the 3- and 4-positions of the thiophene ring are blocked by oxygen in EDOT, minimizing unwanted polymerization at these two β carbon sites. Additionally, the oxygen acts as an electron-donating group, increasing the electron density of the thiophene ring. Therefore, the conjugated polythiophene ring can easily be positively charged by the anion dopants. The opposite side of oxygen atoms is capped by an ethylene moiety to form a stable six-membered ring. This back-bonded ring minimizes the unwanted polymerization reaction branched from the 3- and 4-position. [19~22]

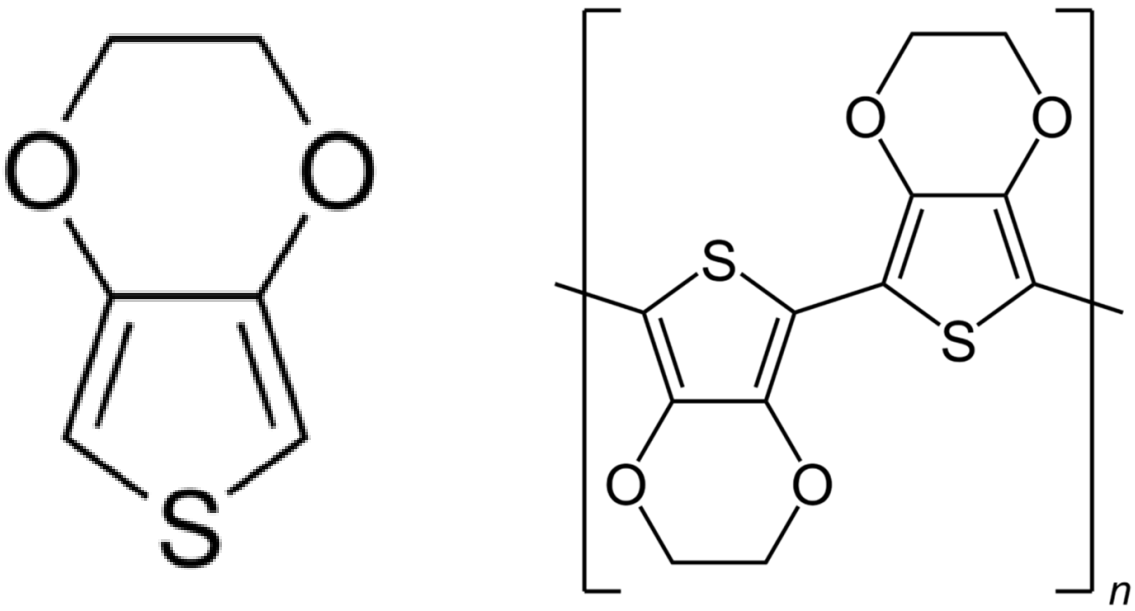

Figure 2 Left: Monomer of PEDOT, 3, 4-ethylenedioxythiophene (EDOT); Right: Molecular structure of poly(3,4-ethylenedioxythiophene) (PEDOT)

The synthesis of PEDOT can be divided into three different types of polymerization reactions: [5]

1. Oxidative chemical polymerization of EDOT-based monomers.
2. Electrochemical polymerization of the EDOT-based monomers.
3. Transition metal-mediated coupling of dihalo derivatives of EDOT.

Chemical polymerization of EDOT can be carried out using several methods and oxidants. The classical method usually employs oxidizing agents such as $FeCl_3$ or $Fe(OTs)_3$. The electrochemical polymerization method has also been successfully used to synthesize high-conductivity PEDOT films but usually a conductive substrate is required. Oxidative polymerization doesn't require a conductive substrate but it is not trivial to reproducibly obtain highly conductive films. Using transition metal-catalyzed coupling of activated organometallic derivatives to prepare PEDOT yields materials with low molecular weight. [1] [5]

Rapidly developing nanotechnology has boosted several advantageous aspects of the synthesized PEDOT materials. Engineering the nanostructure enables high capacitance and superior rate capability of the electrode materials by making much larger electrochemical surface. Thus, great efforts have been devoted to elucidate the controlled synthesis of PEDOT of various nanostructures with enhanced electrochemical properties. Targeting methods have being applied to the synthesis of nanorods, nanowires, nanofibers,

nanotubes or nanocomposite either using template-directed or template-free methods. [23~39] The advantage of template-directed over template free methods is that the materials synthesized from template-directed methods usually have better defined morphology, more uniform size and larger surface area, thus enhancing the electrochemical property of the devices. [27] For example, until now, high aspect ratio (> 200) nanofibers of PEDOT could only be deposited from the vapor-phase, but it has to utilize extrinsic hard templates such as electrospun nanofibers and anodized aluminum oxide. [25] Although solution based chemical and electrochemical deposition methods are much simpler methods, vapor-phase polymerization is the only method to achieve high aspect ratio PEDOT nanofiber up to now. One problem of template directed methods is that it requires postsynthetic template removal, which stifles the development of conducting polymer electronics. [27] Recently, Kaner et al, introduced a simple evaporative vapor-phase polymerization (EVVP) that overcomes these drawbacks and results in vertically directed high aspect ratio PEDOT nanofibers possessing a high conductivity. [25] Their experiment is carried out inside a chemical vapor deposition chamber at ambient pressure. An aqueous microdroplet of oxidant ($FeCl_3$) was placed on a gold-coated substrate and the monomer EDOT was carried under an atmosphere of chlorobenzene vapor. Then they ramped up temperature from 25 to 130 ℃ at the speed of approximate 6.67 ℃/min, and kept at 130 ℃ for 33 min. After 45 mins, they successfully deposited PEDOT nanofibers as a freestanding mechanically robust film. The film can be easily processed into a supercapacitor without using organic binders or conductive additives.

Punya et al. studied the soft template synthesis of PEDOT nanostructures by oxidative polymerization of EDOT in the presence of poly (acrylic acid) (PAA) and $FeCl_3$ which was used an oxidizing agent. [23] The morphology of PEDOT nanostructures revealed flowerlike-shape agglomerates. Their studies revealed that the presence of PAA could only induce a change in morphology during polymerization, but could not influence the molecular structure of the PEDOT nanostructures. Liu and his coworkers reported PEDOT-nanotube synthesis in a porous alumina membrane. [26] The achieved high power capability (25 kW/kg) is attributed to the fast charge/discharge of nanotubular structures: hollow nanotubes allow counter-ions to readily penetrate into the polymer and access their internal surfaces, while the thin wall provides a short diffusion distance to facilitate the ion transport. Impedance spectroscopy shows that nanotubes have much lower diffusional resistance to charging ions than solid nanowires shielded by an alumina template, providing supporting information for the high charging/discharging efficiency of nanotubular structures.

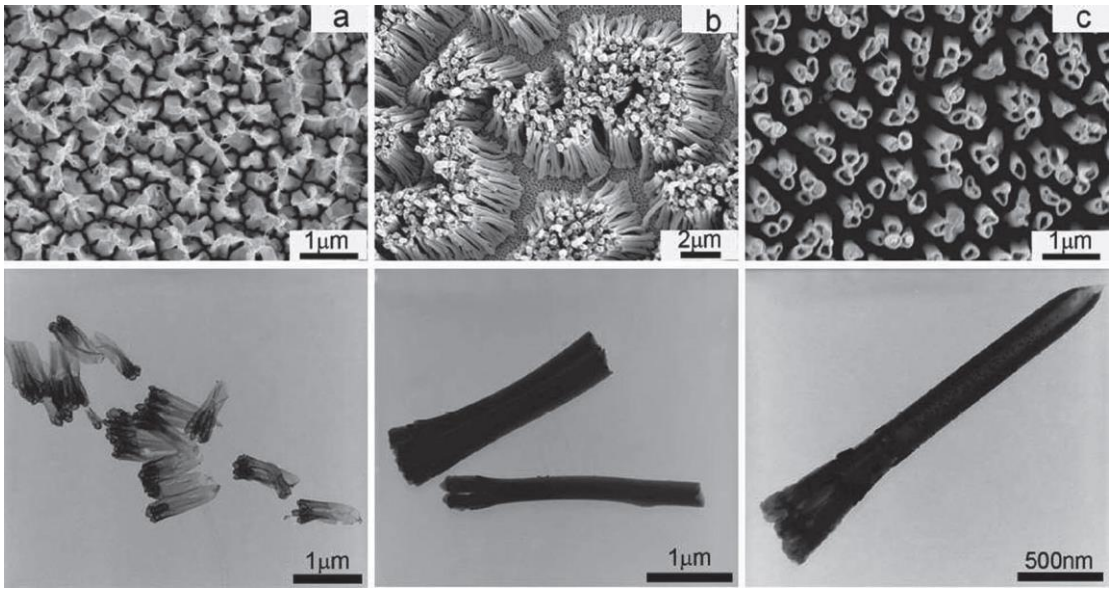

Figure 3. SEM (upper) and corresponding TEM (lower) images of PEDOT nanotubes and nanorods as obtained by template-based growth mechanism at varying oxidation potentials. Adapted with permission from [28]. Copyright 2008, American Chemical Society.

Although PEDOT was initially found to be insoluble in water, an alternative approach to create PEDOT films is the use of "flexible polymer dopants" to make the solution process of conjugated polymers possible. It turns out that using a water-soluble polyelectrolyte (poly(styrene sulfonic acid) (PSS)) currently is the most feasible solution. [29~33] This combination results in a water-soluble polyelectrolyte system with good film forming properties up to a very high conductivity (e.g. 300 S/cm). [34] [35] PEDOT thin films were found to be almost transparent and showed very high stability in the oxidized state. [36] [37] Even heated in air at 100 ℃ for over 1000 h, PEDOT/PSS only undergoes a minimal change in conductivity. [34] [38] In general, these polymers have several redox states with associated control of the electrical conductivity over the full range from insulator to metal. [39]

In addition, PEDOT has been a heavily researched active material for batteries, supercapacitors and solar cells because of its fast change between oxidized and reduced states, as well as a good electric conductivity, ease of synthesis, and low cost. [40] [41] However, despite the intense research efforts, the relationship between synthesis, morphology, doping, and material properties is still poorly understood for PEDOT. With the increasing demand for plastic displays, solar cells and batteries, the need for the flexible and highly conductive materials rapidly increases.

While most researchers focus on the morphology, conductivity and flexibility of the 2-D PEDOT films, [1] [42] [43] our group is interested in 1-D PEDOT nanowires encompass interesting properties compared with films due to larger surface area and quantum confinement. In particular, I will be preparing PEDOT nanowires via lithographically patterned nanowire electrodeposition (LPNE), and then characterizing the nanowires using atomic force microscope (AFM), electrochemical impedance spectroscopy (EIS), cyclic voltammetry, and chronoamperometry.

PEDOT nanowires are reported to be more conductive than PEDOT thin films, a rather surprising observation that has yet to be explained. [44~46] Various synthesis parameters (electrodeposition method, supporting electrolyte, solvent, etc.) can affect the nanowire properties (conductivity, morphology, etc.). Further, to better understand this phenomena in both macro and micro scale, I will use EIS and Raman spectra to study the mechanism of the conductivity change.

1.3 Lithographically Patterned Nanowire Electrodeposition

Lithographically patterned nanowire electrodeposition (LPNE), which was developed by Penner's group is a feasible method to synthesize noble-metal, semiconductor and conducting polymer nanowires on glass or oxidized silicon surfaces. [47~49] As shown in Figure 4, this method requires the preparation of a sacrificial nickel nanoband electrode

using optical lithography and the subsequent electrodeposition of a desired nanowire at this electrode. When we electrodeposit a nanowire into this 'nanoform', a wire with a rectangular cross-section is produced, where the thickness is determined by the height of the nickel and the width is generally controlled by the deposition time. The optical diffraction limit constrains the spacing between nanowires as we use optical lithography to define the position of the nanowires on the substrate. The position of nickel nanoband electrodes prepared in the first four steps of the LPNE process shown in Figure 4 determines the position of nanowires on a glass surface. Nitric acid etching can remove the exposed nickel electrochemically in several minutes depending on the thickness and width of nickel. We continue nickel oxidation until we etch nickel at the exposed edges of this pattern, undercutting the photoresist by 100–300nm. Nickel 'overetching' produces a horizontal trench into which we electrodeposit a desired nanowire in step 5 (Figure 4).

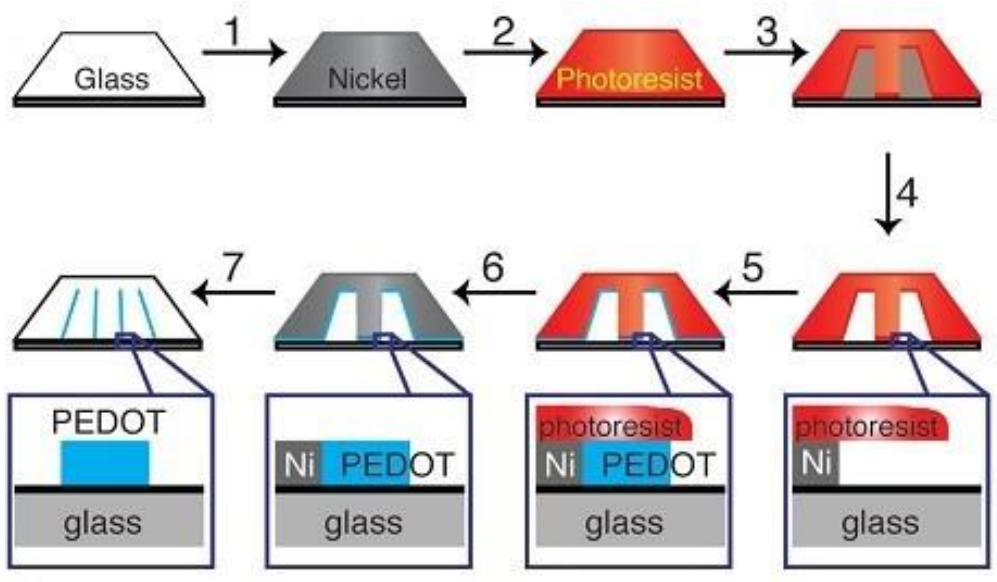

Figure 4. Lithographically patterned nanowire electro-deposition (LPNE) method to synthesize

PEDOT nanowire.

2. Experimental

2.1 Chemicals

The monomer 3,4-ethylenedioxythiophene (EDOT), acetone, lithium perchlorate were purchased from Aldrich and used as received. The Millipore MilliQ water (ρ>18.0 MΩ•cm) was used to prepare all solutions. 0.8 mol/L nitric acid used for the etching of nickel layer was prepared by diluting nitric acid (purchased from Aldrich) with the pre-calculated volume of distilled water. Positive photoresist and developer were both obtained from Rohm and Hass. Nickel rod (99.995% pure) was purchased from Kurt J. Lesker company, premium microscope slides were obtained from Fisher Scientific Company, L.L.C. and liquid nitrogen was purchased from Praxair.

2.2 Equipment

2.2.1 Denton Vacuum BTT-IV

The physical vapor deposition device, Denton Vacuum BTT-IV was purchased from Denton Vacuum, Inc. It is mainly used for the nickel layer deposition on the glass slides.

Figure 5. Denton Vacuum BTT-IV for Physical Vapor Deposition

2.2.2 SQM-160 Thin Film Deposition Monitor

The SQM-160 was purchased from INFICON. It was used for measuring rate and thickness in the thin film deposition processes. Sensor inputs can be assigned to different materials, averaged for accurate deposition control.

Figure 6. SQM-160 Thin Film Deposition Monitor

2.2.3 OAI Model 30 UV light

The UV Light is provided by the OAI Model 30 (shown with optional stand), which was purchased from OAI, Inc. It consists of a stand-alone light source, a constant intensity controller, and a shutter timer. This UV light source is available in various beam sizes up to 24 inches square with output spectra ranging from 220 nm to 450 nm, using the appropriate lamp.

Figure 7. Light source for photolithography: OAI Model 30 UV light

2.2.4 Electrochemical Cell

Electrochemical polymerization and measurements of PEDOT were performed by using a

one-compartment, three-electrode electrochemical cell. A Pt electrode, with area A = (1 × 1) cm^2, a standard Ag/AgCl electrode and the glass slide coated with nickel strips have been used as counter electrode, reference electrode and working electrode, respectively to perform electrochemical studies and to prepare nanowires for morphological and Raman characterization.

The electropolymerization and deposition of PEDOT were carried out using cyclic voltammetry (CV) and chronamperometry starting from unstirred solutions containing 2.5 mM EDOT monomer and 12.5 mM lithium perchlorate (Li_3ClO_4).

Figure 8. The set-up of the three electrode electrochemical cell

2.2.4 Characterization Tools

The morphology of the electrodeposited nanowires was analyzed by atomic force microscopy (AFM, Solver P47H, NT-MDT, Russia). AFM characterization was performed in the standard semi-contact mode. The AFM tip (HQ:NSC14/HARD/AL BS) was

purchased from μmash. It has a typical probe tip radius of 8 nm. AFM images were collected in air and at room temperature.

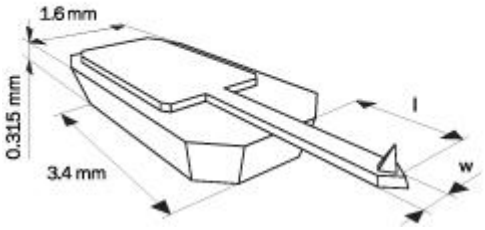

Figure 9. Left: Schematic drawing of the cantilever Right: SEM image of the cantilever

The Raman Spectroscopy used for PEDOT characterization was from Prof. Anne Kelley's group in UC Merced. Excitation for Raman spectroscopy was provided by a Coherent Innova 90C-5 argon ion laser which can produce cw radiation at several discrete visible wavelengths between 458 and 514 nm. Beam diameter is about 1 mm. Jobin-Yvon T64000 Raman microscope system provides the imaging of the samples and laser spot, which consists of the following basic components:

1). A modified microscope which focuses the incoming laser light onto the sample and collects the Raman scattered light.

2). A triple spectrometer composed of a "subtractive double" premonochromator coupled to a single spectrograph.

3). A CCD (charge-coupled device) detector which converts photons to electrons that can be read out by the computer.

4). The J-Y software program LabSpec runs the CCD detector which reads out the Raman

scattered light, and moves the gratings in the instrument which determine what wavelengths reach the detector.

The PARSTAT 2273 from Princeton Applied Research Company is utilized for the electrochemical impedance spectroscopy study of synthesized PEDOT nanowires from 1 Hz to 1MHz.

Figure 10. PARSTAT 2273 from Princeton Applied Research Company for electrochemical impedance spectroscopy study of PEDOT nanowires.

2.3 Experimental Procedure

2.3.1 Synthesis of PEDOT Nanowires

The seven-step LPNE procedure is implemented shown as follows. [47~49]

a) *Glass slides Cleaning*: soda-lime glass microscope slides were diced into 1×1 squares and then the squares were submerged into the aqueous Nochromix solution for 24 h for deep cleaning and then air dried.

b) *Nickel Layer Deposition*: we physically deposited a 40-nm-thick nickel film (ESPI, 5N purity) by hot-filament evaporation at a rate of around 0.7 $A^{\circ}s^{-1}$. The film thickness and evaporation rate were monitored by SQM-160.

c) *Photoresist Coating*: the nickel-covered glass squares were then coated with a positive photoresist layer (Shipley 1808) by spin coating. We put a 1 ml photoresist onto each square and then rotate the square at 2,500 r.p.m. for 80 s. We soft-baked freshly coated squares at 90 ◦C for 30 min. This produced a photoresist thickness of ~0.8 μm.

d) *Developer Treatment*: After cooling to room temperature, we placed a transparent contact mask onto the photoresist with a quartz plate and exposed this masked surface to the OAI light source, with an output power of 0.5 mW/cm^2 for 3.3s. We then soaked the slide first in a developer–water solution (Shipley MF-24A) for 30 s, and then wash the slide in pure water, before drying in a stream of air.

e) *Nitric Acid Etching*: Etch the slides with 0.8 M nitric acid for 8 mins to remove the expose nickel and rinse it with pure water.

f) *Electrodeposition of PEDOT*: A one-compartment, three-electrode electrochemical cell was used to electrodeposit PEDOT nanowires. The glass slides with nickel bands and trenches was the working electrode. Both the stripping and deposition were carried

out on a computer-controlled Gamry Instrument potentiostat/galvanostat. Cyclic voltammetry and chronamperometry were utilized for preparation of PEDOT nanowires and comparison of the resulting nanowires. The setting of the electrodeposition is shown in figure 11 and 12.

g) *Substrate Cleaning*: finally the glass squares were rinsed with electronic grade acetone to remove the photoresist and then submerged in 0.8 M nitric acid for 8 mins. After that, the glass squares were rinsed with Nanopure water and dried with air.

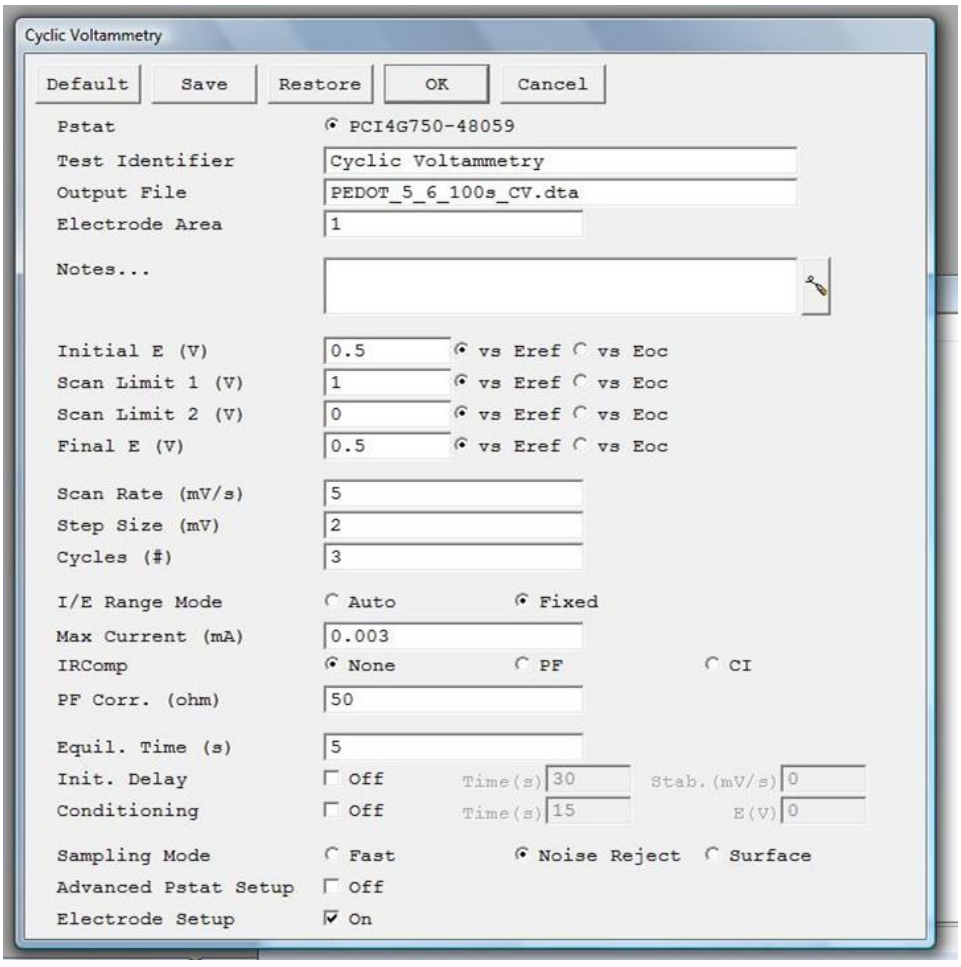

Figure 11. Cyclic voltammetry setting for PEDOT synthesis

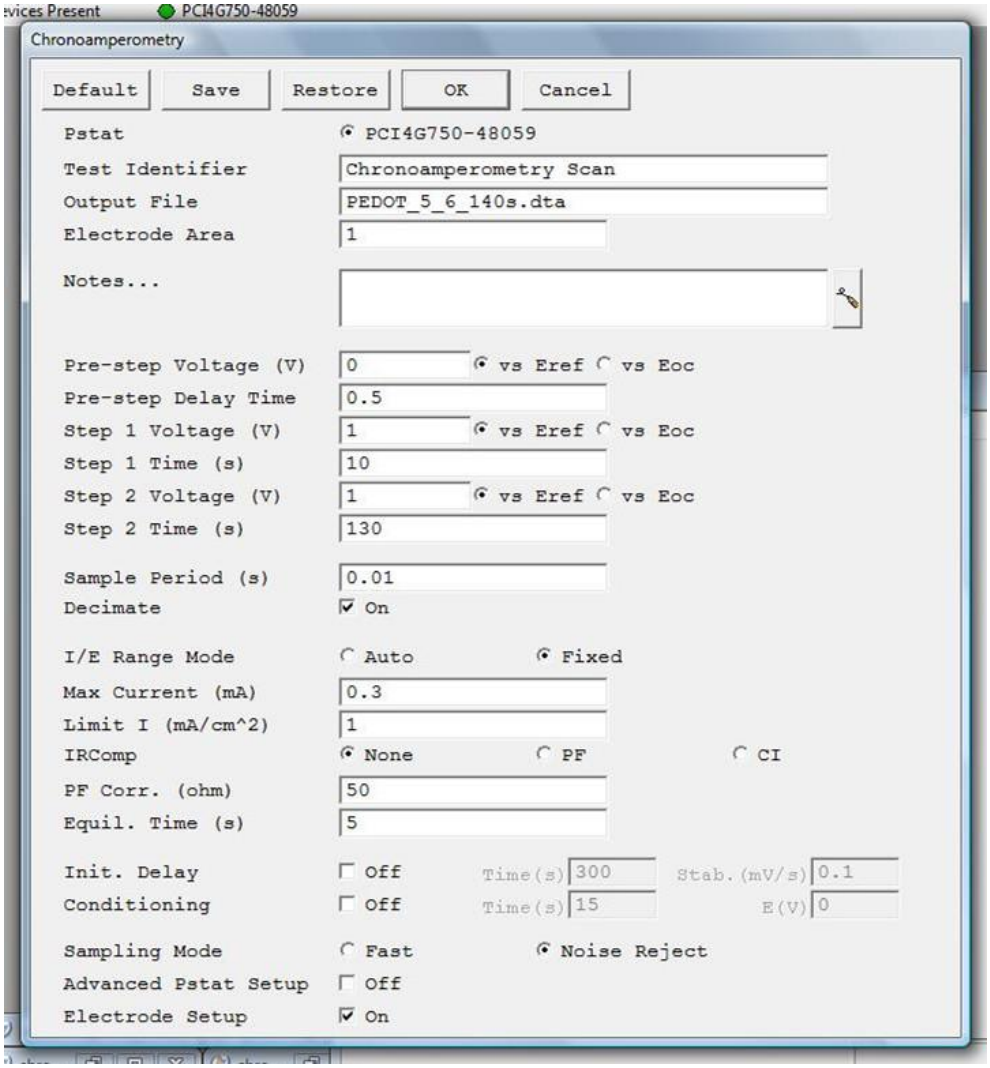

Figure 12. Chronoamperometry setting for PEDOT synthesis

2.3.2 Conductivity Measurement of PEDOT Nanowires

The procedure to electrodeposit PEDOT nanowires for conductivity measurement is generally the same as the steps listed in session 2.3.1, except the mask we are using for photolithography (1 mm spacing this time). After the nanowires which have 1 mm spacing were synthesized, I washed away the photoresist with acetone and then spin coat again under the same condition. The glass slides were put in the oven which was set at the

temperature of 90 ℃ for 30 mins. Then a transparent mask which contains only one 200-nm wide line was used to create a pattern. Afterwards, I soaked the glass slide in the developer for 30 seconds and 0.8 M nitric acid for 8 mins. By finishing the nitric acid etching, the single PEDOT nanowire was connected by Nickel bands on both sides. In order to enlarge the contacting area, silver paste was dipped on the Nickel bands. After the silver paste is dried, a simple multimeter can measure the conductance of PEDOT nanowire.

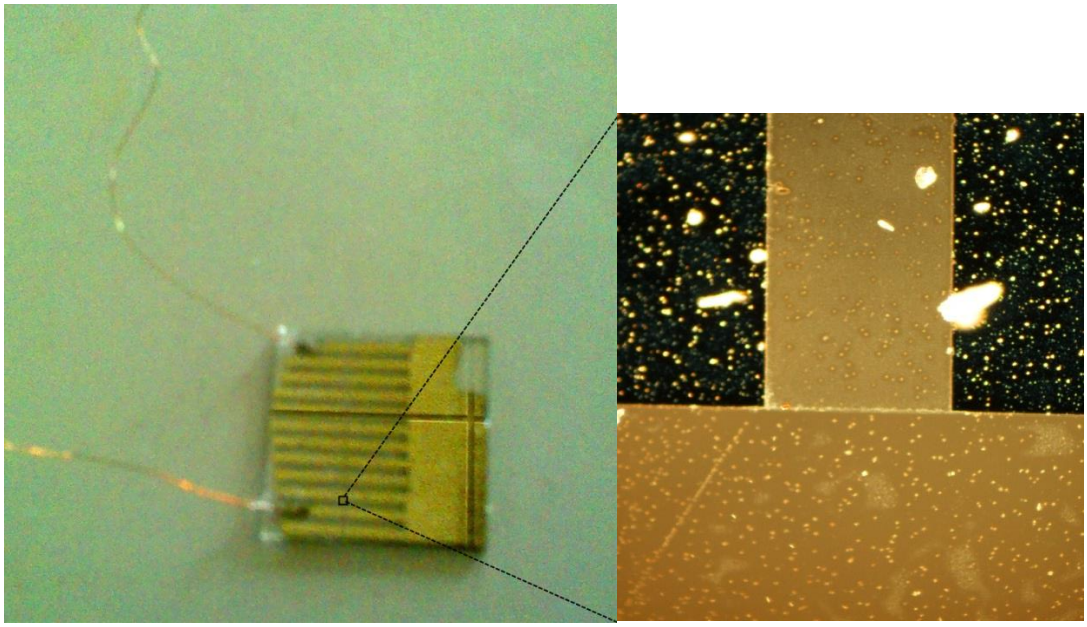

Figure 13. Left: Image of how I measured the conductivity of a single PEDOT nanowire. Each nickel band connected with one single PEDOT nanowire (originally two but I cut off one) and a thin copper wire is glued to the nickel band with silver paste. Right: Microscopic image of the area using the magnification of 100 in which the single nanowire is connected by two nickel bands.

2.3.3 Raman Spectroscopy Measurement of PEDOT Nanowire

The wavelength of Raman spectroscopy was 488 nm and the excitation power at the

sample was 0.2-0.3 mW. The Raman microscope was first used as an ordinary light microscope, viewed with a video camera, to identify the nanowires and position the focused laser spot onto a wire. The Raman spectrum was then collected using an integration time of 120 s. The spectral resolution was about 5 cm^{-1}.

3. Results and Discussion

3.1 Impact of Electrodeposition Methods

Both cyclic voltammetry and chronoamperometry are utilized to electrodeposit PEDOT nanowires. Figure 14 shows the cyclic voltammogram of the EDOT electropolymerization from the aqueous solution with 12.5 mM lithium perchlorate as the electrolyte. The voltage window is 0.4 V to 1.05 V vs standard Ag/AgCl reference electrode and the sweep rate is set as 20 mV/s for 5 cycles. The first cycle as you can see in the graph has much larger current than the other four cycles. That can be explained by the fact that when it is bare nickel contacting the solution, electron donation of the monomer EDOT can be done much faster. As the nickel band is gradually being covered by polymer, the electron transfer becomes sluggish and stable, which is demonstrated by the overlap of the cyclic voltammogram from the second to the fourth cycle.

With the aim to obtain more information about the polymerization process of EDOT, a set

of electrodeposition in the potentiostatic mode at different potentials has been performed. A typical potential static curve for the electrodeposition of PEDOT nanowire is shown in figure 15. The deposition voltage is 1.0 V vs standard Ag/AgCl reference electrode and the deposition time is 300 seconds, which is comparable to the total time in cyclic voltammetry.

The resulting PEDOT nanowires synthesized from the cyclic voltammetry and chronoamperometry methods are both characterized by the optical microscopy. The preliminary results show that the deposition methods have an impact on the width and morphology of the nanowires. The magnitude of the optical microscopy is set as 100×/0.8. As we can see from the images of the synthesized nanowires, those electrodeposited PEDOT nanowires are a light blue color, which is the color of oxidized PEDOT. Experiments show that when PEDOT nanowires approach a micrometer in width and height, this blue color can be seen in optical microscopy. So we can ascertain that these nanowires are over one micrometer in width although it is hard to precisely measure the width of PEDOT nanowires. By comparison between the PEDOT nanowires synthesized via cyclic voltammetry and potential static method, which are shown in figure 16 and figure 17, we can conclude that chronoamperometry produces more uniform and wider nanowires. The obvious explanation is that:

1. PEDOT nanowires synthesized via chronoamperometry accumulates more charge so that more EDOT monomers can be oxidized and polymerized to form PEDOT nanowire;

2. The stable current is a sign of relatively constant oxidizing speed of the monomer EDOT, which is obviously beneficial to the uniform structure of the resulting PEDOT nanowire. Conduct polymer can be synthesized through both CV and chronoamperometry methods utilizing the micro nickel electrode.

We also characterized the resulting PEDOT nanowires via atomic force microscopy (AFM). We can see from figure 18 that the size and width of the PEDOT nanowires are well confined. LPNE leverages conventional microfabrication methods to produce a horizontal trench with a width of about 600 nm terminated by a vertical nickel electrode. Immersion of this trench into an aqueous solution of EDOT permitted growth of a PEDOT nanowire by oxidative electropolymerization at the nickel electrode and within the confines of this trench. This method provided for independent control over the thickness and width of the nanowire while also enabling the synthesis of PEDOT nanowires that were millimeters in total length.

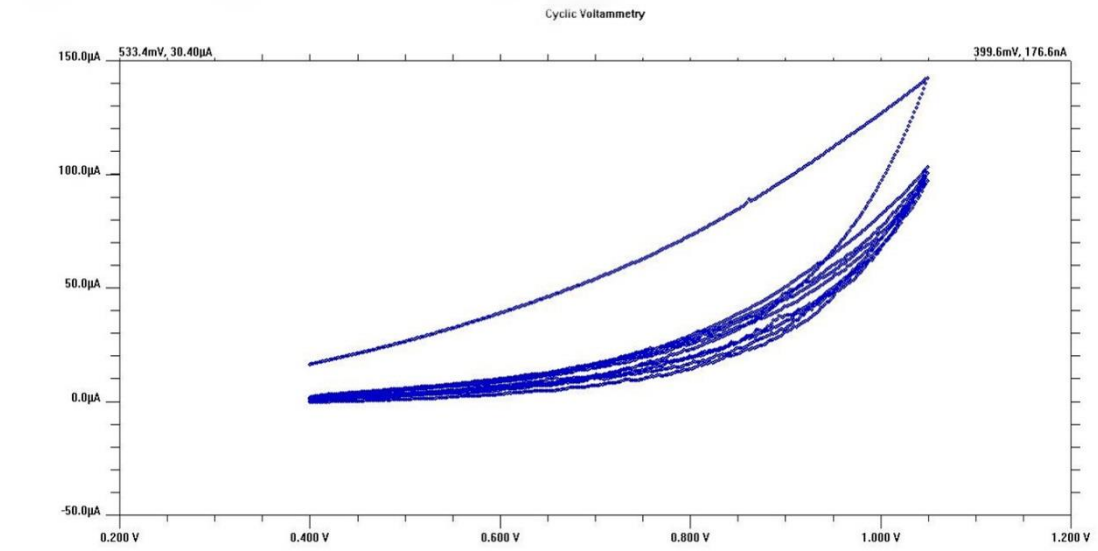

Figure 14. Cyclic voltammetry (CV) curve for the electrodeposition of PEDOT nanowire. The voltage window is 1.05 V to 0.4 V vs SCE, sweep rate set as 20 mV/s and 5 cycles

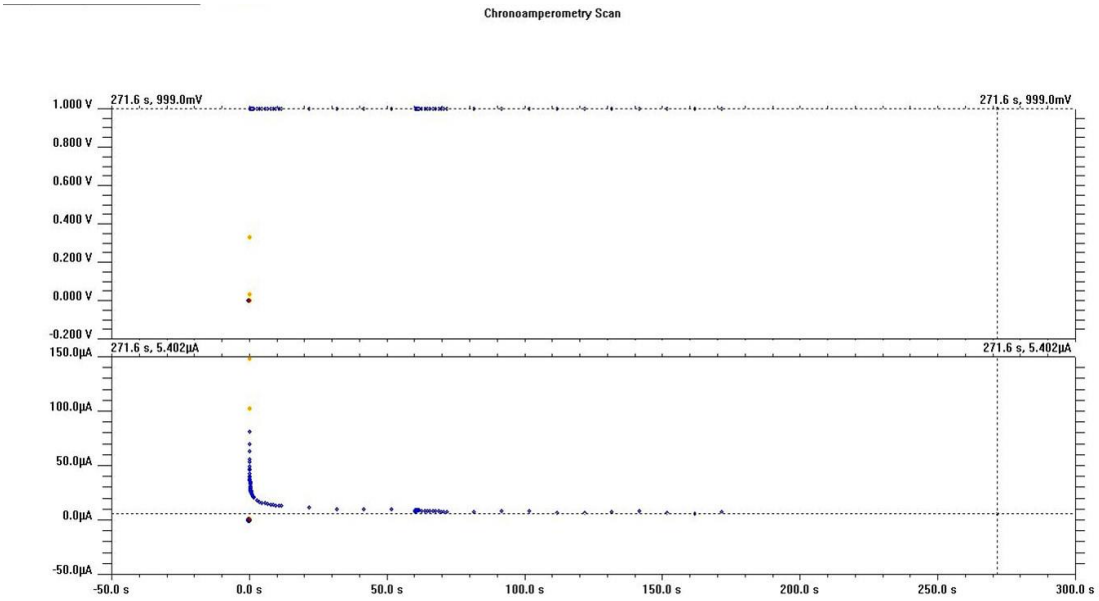

Figure 15. Potentiostatic curve for the electrodeposition of PEDOT nanowire in which 1.0 V vs SCE and 300 s were used.

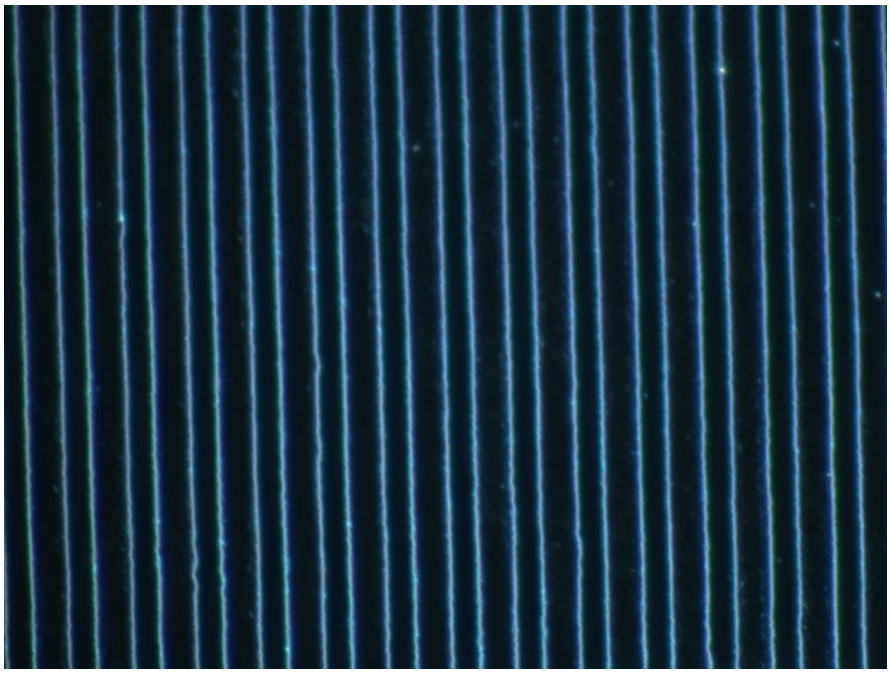

Figure 16. The nanowires grown under CV, seen from the microscope using the magnification 100

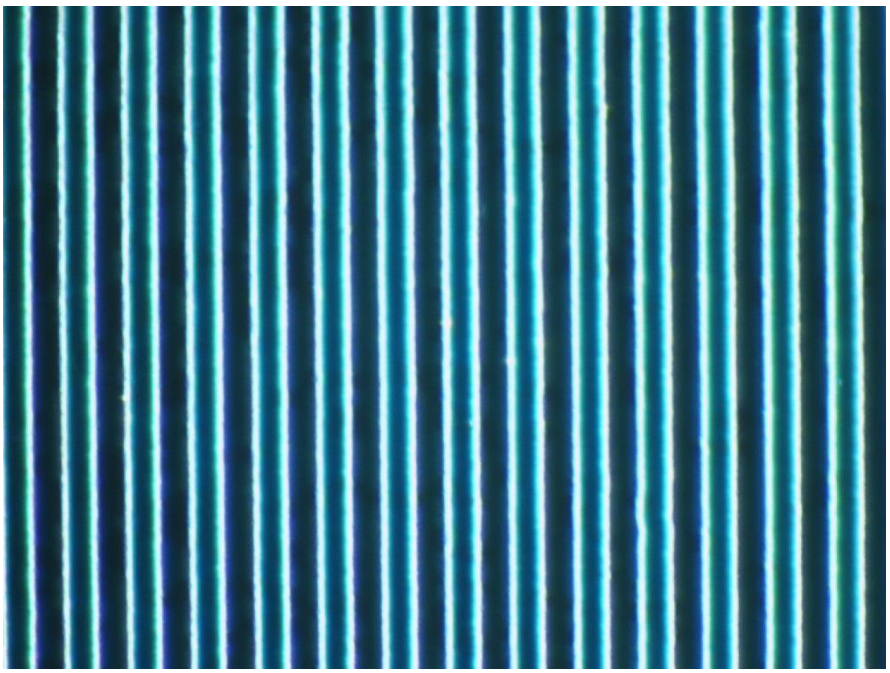

Figure 17. The nanowires grown under chronoamperometry, seen from the microscope using the magnification 100

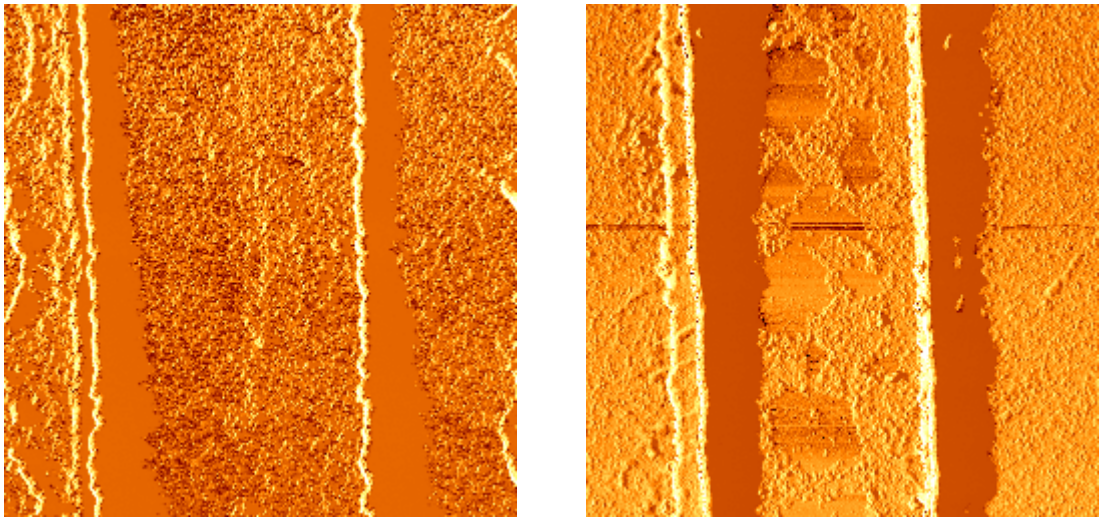

Figure 18. Left: 5μm×5μm AFM image of PEDOT nanowire synthesized with cyclic voltammetry Right: 5μm×5μm AFM image of PEDOT nanowire synthesized with chronoamperometry.

3.2 Impact of Electrodeposition Voltage and Time

From the above results, chronoamperometry is more favorable for the polymerization of the uniform PEDOT nanowires. So in the following study, we used chronoamperometry to synthesize PEDOT nanowires in different conditions.

Emanuela et al, synthesized PEDOT via cyclic voltammetry and in their cyclic voltammgram of the electropolymerization in 0.1 nM NaPSS, two oxidation peaks can be observed. One peak is localized at 1.15 V and the other is at 1.40 V. In particular, the latter peak is shifted toward lower potentials in the following cycles. [50]

However, there is no obvious oxidation and reduction peak showing in our cyclic

voltammetry curve. Thus the optimal voltage for the electrodepostion of PEDOT nanowires via potential static method is not well clarified. In order to optimize the deposition voltage, a set of experiments was conducted in which 0.4 V, 0.6 V, 0.8 V, 1.0 V, 1.05 V is applied as the deposition voltage. The deposition curve for each deposition voltage is quite similar to the one shown in figure 15. The deposition current for each voltage is decreasing rapidly in the first few seconds and became stable afterwards. Usually the stable deposition current is around 2 μA.

As you can see from figure 19, the PEDOT nanowires seem to grow wider and more uniform as the deposition potential increases and when the voltage drops down to 0.4 V, nearly no continuous nanowire was observed. No obvious difference is observed for the nanowires grown under 1.0 V and 1.05 V. The voltage cannot increase to more than 1.1 V due to the voltage window of the aqueous solution. Thus it is concluded that 1.0 V is the optimized electrodeposition voltage.

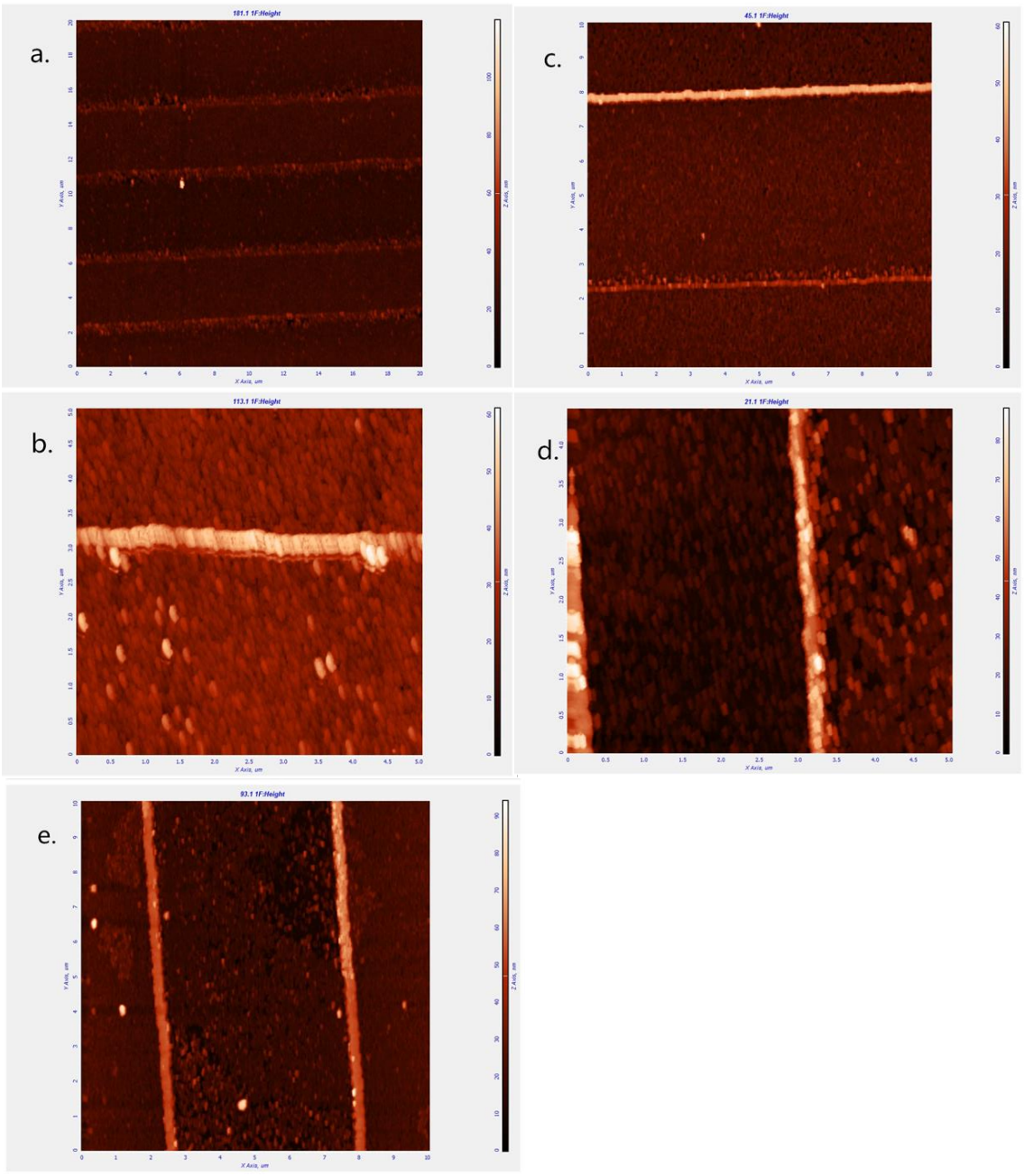

Figure 19. AFM image of PEDOT nanowire synthesized using potential static with (a) 0.4 V, (b) 0.6 V, (c) 0.8 V, (d) 1.0 V, (e) 1.05 V as the deposition voltage

In order to correlate the relationship between deposition time and size of the nanowires, a series of experiments was conducted. We set the deposition time ranging from 20 s to 120 s and using the same electrodeposition condition. The results are shown in figure 20.

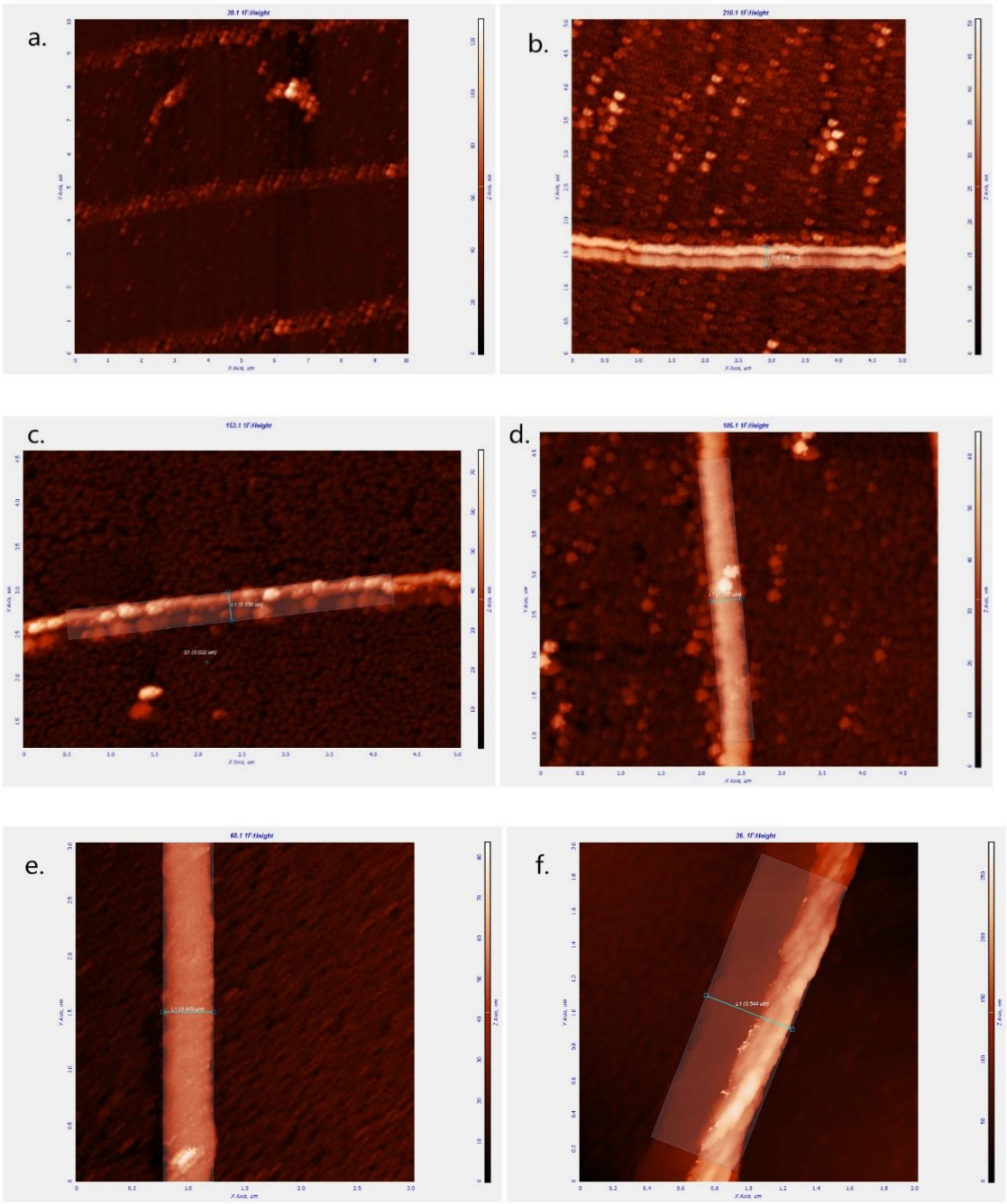

Figure 20. AFM image of PEDOT nanowire synthesized using potentiostatic method under the deposition voltage of 1.0 V and deposition time (a) 20s, (b) 40s, (c) 60s, (d) 80s, (e) 100s, (f) 120s.

The obvious trend is that as the deposition time increases, the width of the PEDOT nanowire increases. The atomic force microscopy is used to measure the width of the nanowires. Table 3 summarized the deposition time and the width of the synthesized

PEDOT nanowire. We can see that, except the case of 20s (no noticeable nanowire grow) and 120s (overgrown), a linear relationship between the deposition time and the growing width of the nanowires is observed.

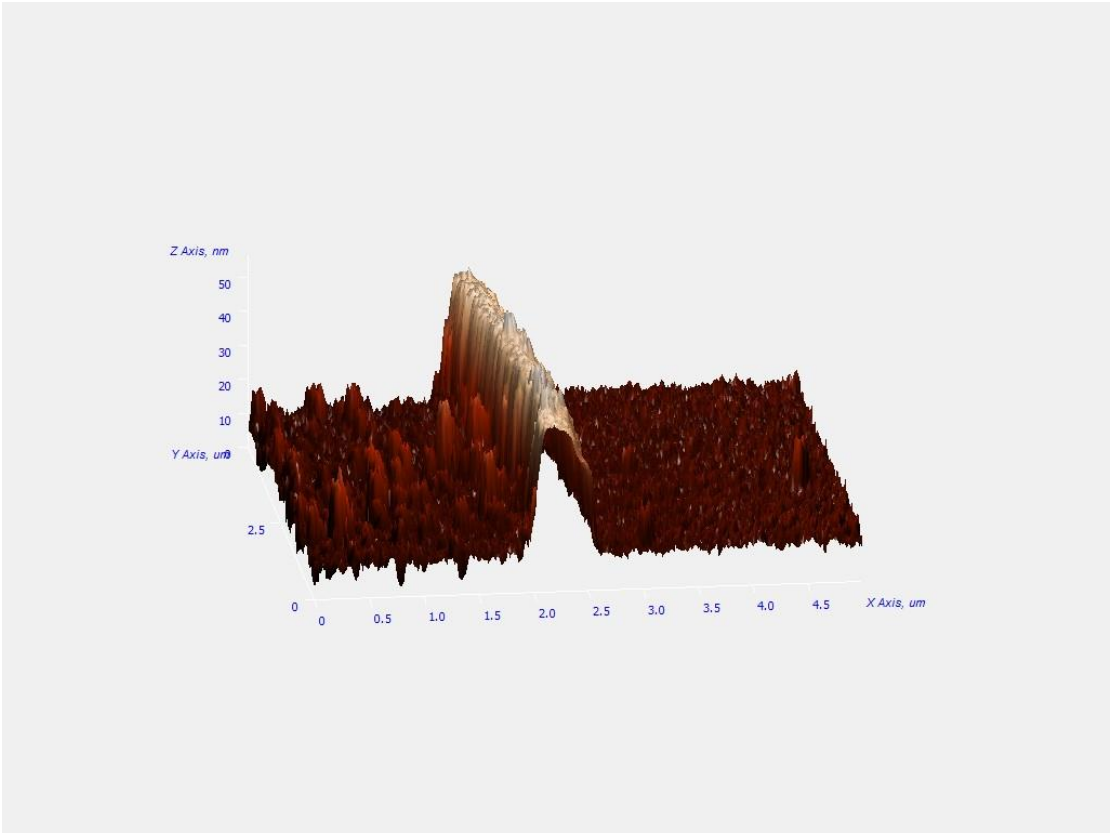

Figure 21. 3D AFM image of PEDOT nanowire synthesized using potential static method under the deposition voltage of 1.0 V and deposition time 100s.

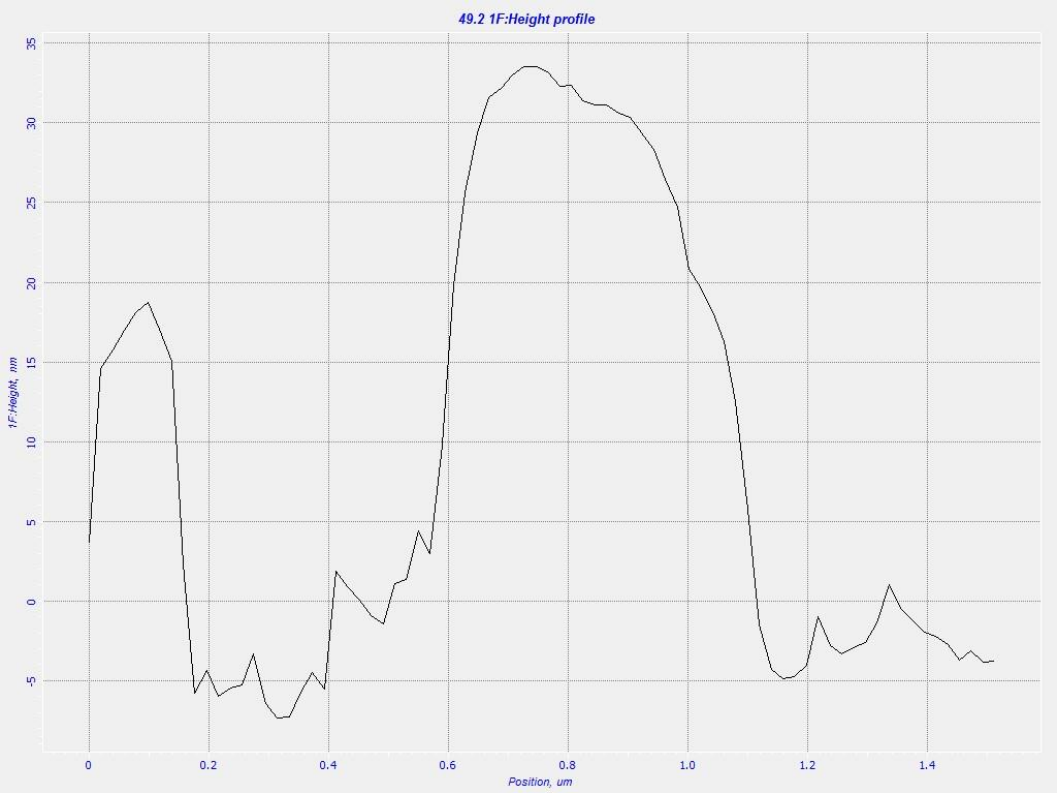

Figure 22. AFM height measurement of PEDOT nanowire synthesized using potential static method under the deposition voltage of 1.0 V and deposition time 100s.

Time (s)	Height (nm)	Width (nm)
20	40	N/A
40	40	150
60	40	330
80	40	387
100	40	530
120	40	544

Table 3. The width and height measurements of the PEDOT nanowires synthesized under different deposition time

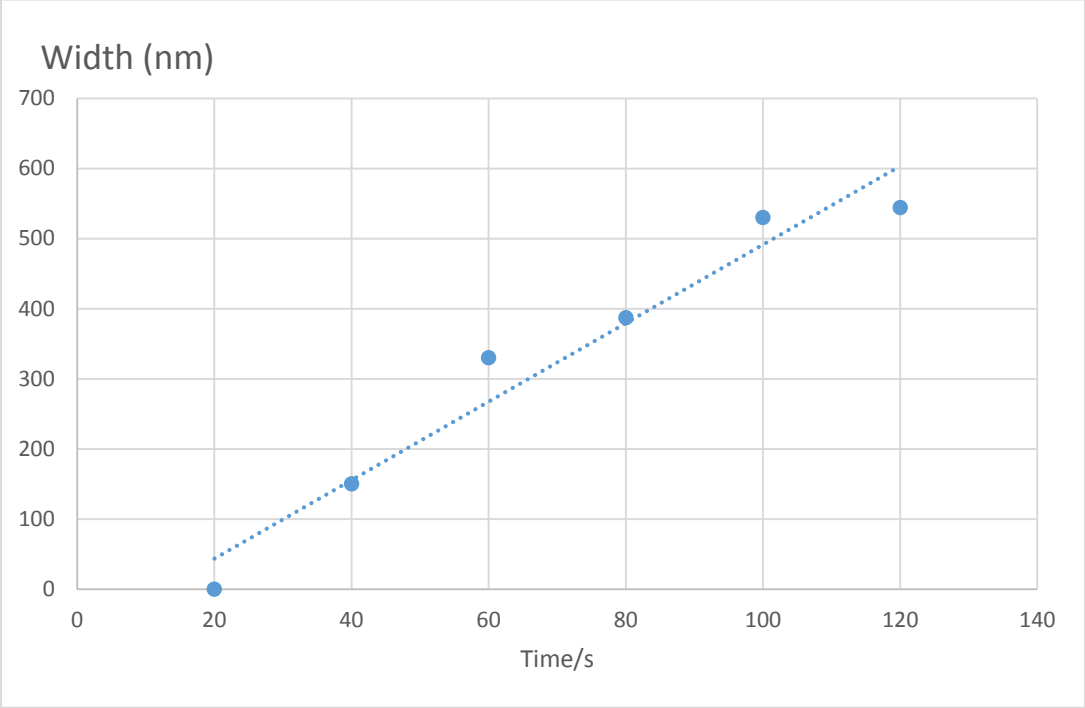

Figure 23. Linear regression of the width of synthesized PEDOT nanowires and the deposition time.

3.3 Conductivity Measurement of PEDOT Nanowires

Conductivity is one key feature of conducting polymers as it enables PEDOT a number of potential applications for the electronics industry. From the published results in the past several decades, the conductivity of PEDOT can vary orders of magnitude. [42] [43] [44] [45] [46] [51] There have been a lot of research groups reporting various schemes to improve the conductivity of PEDOT. [45] [46] Recently, Winther-Jensen reported PEDOT thin film deposition in which the EDOT monomer was introduced in the vapor phase, resulting in reported conductivities as high as 1000 S/cm. [52] This method used spin-coating of the oxidizing agent of iron toluensulfonate. Meng also introduced a CVD process using

chlorinated EDOT for PEDOT. [53] Building on the idea of introducing the EDOT from the vapor phase, Lock developed an oxidative chemical vapor deposition (oCVD) method which employs the sublimation of the oxidizing agent of iron(III) chloride, obtaining a maximum conductivity of 105 S/cm. PEDOT synthesized from chemical oxidization via iron (III) tosylate can reach a conductivity of over 1000 S/cm while it is only 0.075 S/cm if PEDOT is oxidized by $Ce(SO_4)_2$. [54]

In order to get a better knowledge of the electrical property of the synthesized PEDOT nanowires, the conductivity of individual nanowires was measured.

There have been several reports about the conductivity measurement of semiconductor nanowires. [55~57] For example, S. Murali et al. used the powder solution composite (PSC) method to obtain the conductivity of ZnO nanowires from impedance spectroscopy measurements of ZnO nanowires dispersed in solution. [55] They calibrated PSC method by comparing impedance spectroscopy measurements of ZnO powder dispersed in solution with four-point probe measurements on bulk ZnO ceramic pellets. Conductivity values for ZnO nanowires obtained using this novel approach were found to be comparable to reported values obtained using two-point and four-point probe measurements of single or multiple nanowire devices isolated on a substrate. Long et al. alternatively utilized platinum microleads to measure the electrical properties of a single CdS wire. [56] They first ultrasonically dispersed CdS nanowires in ethanol, then placed a drop of dilute solution on an insulating SiO_2/Si substrate. After the solution was dry, they

used an electron microscope to find an appropriate nanowire on the substrate, then platinum (Pt) microleads 1.0μm in breadth and 0.8μm in thickness were fabricated on the single wire by using a focused ion beam.

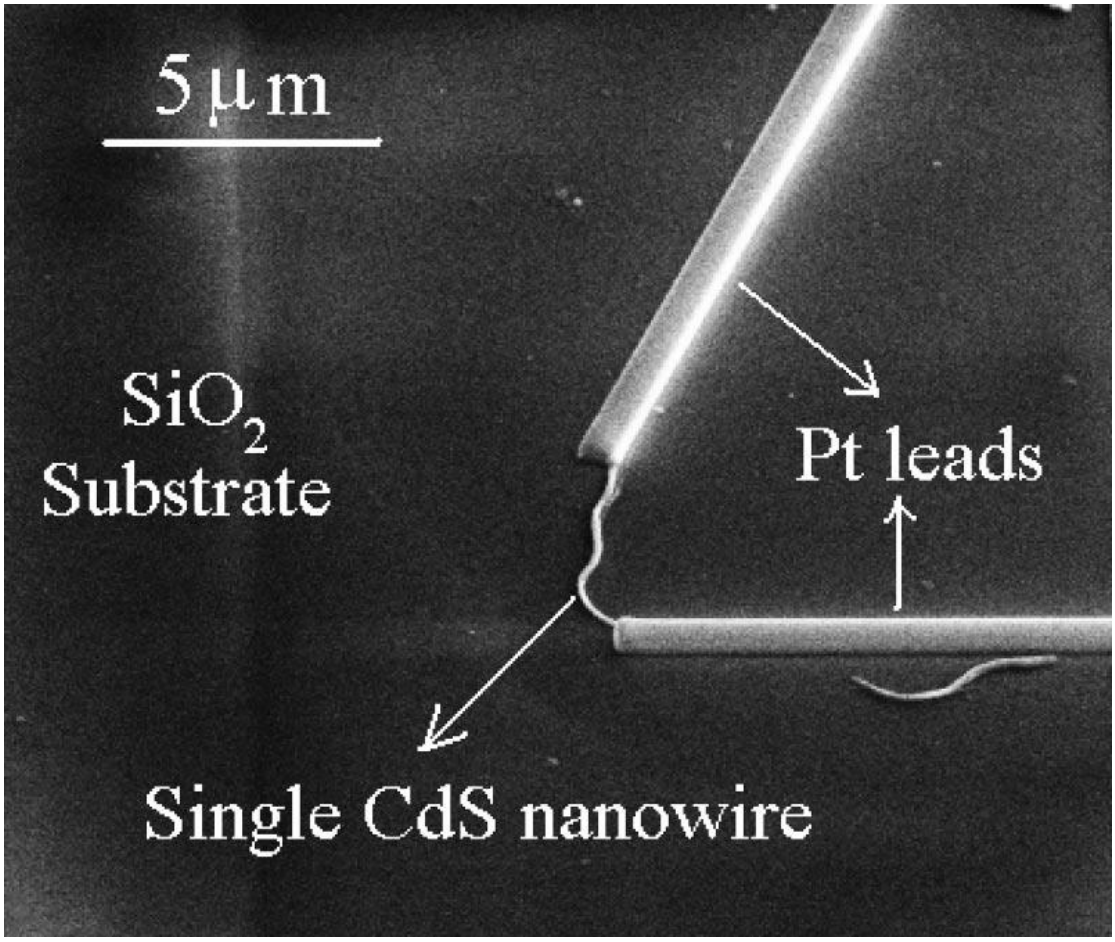

Figure 24. SEM image of the single CdS nanowire and a pair of Pt micro-leads fabricated with focused ion-beam deposition. Reference [56]

The method our lab used is somewhat similar to the second method mentioned above. At first, lithographically patterned nanowire electrodeposition method is used to synthesize the 1 mm spacing nanowires. Instead of nitric acid etching of the remaining Nickel after washing away the photoresist with acetone, I spin coated another layer of photoresist in order to create another pattern. The mask I used this time is the one contains only one

perpendicular 100 nm wide trench so that by etching the nickel layer with nitric acid, there would be 100 nm wide PEDOT nanowire with two tips contacted with nickel band. The conductance of the PEDOT nanowire is measured by scanning through voltages and measuring the current in the meantime. Then atomic force microscopy is utilized to measure the accurate width, height and length of each single nanowire. After all this information is known, the conductivity of each single nanowire can be calculated using the Rohms equation ($\sigma = \frac{L}{R*A}$), where R is the electrical resistance of a uniform specimen of the material (measured in ohms, Ω), L is the length of the piece of material (measured in centimeters, cm) and A is the cross-sectional area of the specimen (measured in square centimeters, cm^2).

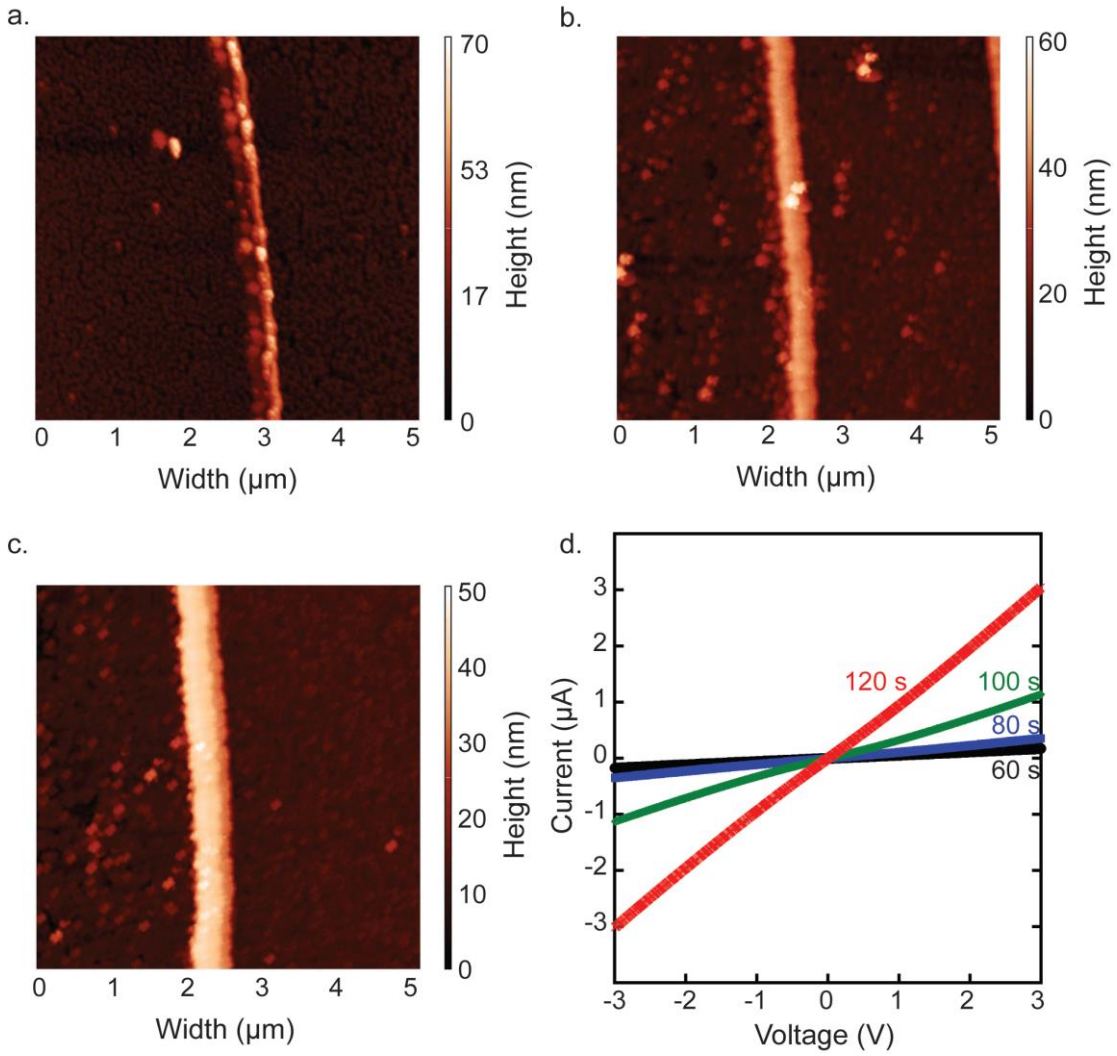

Figure 25. 5 um x 5 um AFM image showing a single PEDOT nanowire prepared after 60 seconds of deposition, b) 5 um x5 um AFM image showing a single PEDOT nanowire prepared after 80 seconds of deposition, c) 5 um x5 um AFM image showing a single PEDOT nanowire prepared after 1000 seconds of deposition, d) Current-voltage curves of single, 200um long PEDOT nanowires grown for 60s (black), 80s (blue), 100s (green), and 120s (red).

Table 4. PEDOT Nanowire Dimension vs. Room Temperature Conductivity

Time (s)	Height (nm)	Width (nm)	Conductivity (S/cm)
60	50	330	7
80	50	387	12
100	50	490	29
120	80 (Overgrow)	700	35

Table 5. PEDOT Nanowire Dimension vs. Conductivity from reference [44]

Height	Width	Conductivity (S/cm)
48 nm	582 nm	39.6
80 nm	440 nm	11.7
90 nm	205 nm	7.6
60 nm	340 nm	6.6
30 nm	1 mm	9.3
150 nm	180 μm	13.0
45 nm	1.5 mm	9.3
170 nm	312 μm	3.1
75 nm	75 nm	9.4
100 nm	100 nm	66
120 nm	120 nm	92
145 nm	145 nm	106
170 nm	170 nm	38

Electrochemical deposition is an excellent synthesis method for achieving systematic control of electrical conductivity over a wide range of values. The measured conductivity of PEDOT polymer nanowires grows dramatically as the deposition voltage and

deposition time increases. The range of conductivity achieved was from 1 S/cm to a high of 40 S/cm. The data from table 5 are also in accord with our conductivity measurements of PEDOT nanowires of different sizes and morphology. As the height and/or width changes, the resulting conductivity changes in the range of 3.1 S/cm to a high of 106 S/cm. Thus it would be of great importance to study why the conductivity of PEDOT nanomaterials changes.

3.4 Proposed Explanations for Conductivity Change

In traditional conducting materials such as metals, their valence electrons are generally free to move and they can travel through the lattice that forms the physical structure. So the conductivity of metals usually remains in a certain range. However, unlike those traditional materials, the conductivity of conducting polymer changes dramatically as the synthesis conditions changes. [44~46] The observed conductivities are completely consistent with our preliminary analysis that PEDOT with longer conjugation length and higher doping level has a higher electrical conductivity. [58] The extreme complexity of electrical conductivity of conducting polymer makes the true nature of conductivity unclear since the electrical conductivity is a collective function of not just the conjugation length and doping level but also crystallinity, interface with the substrate, and the measurement conditions, such as frequency and temperature. In figure 26, the polymerization process of PEDOT is shown. It is basically an oxidization polymerization process which involves the donation of one electron of each monomer EDOT and the further doping process.

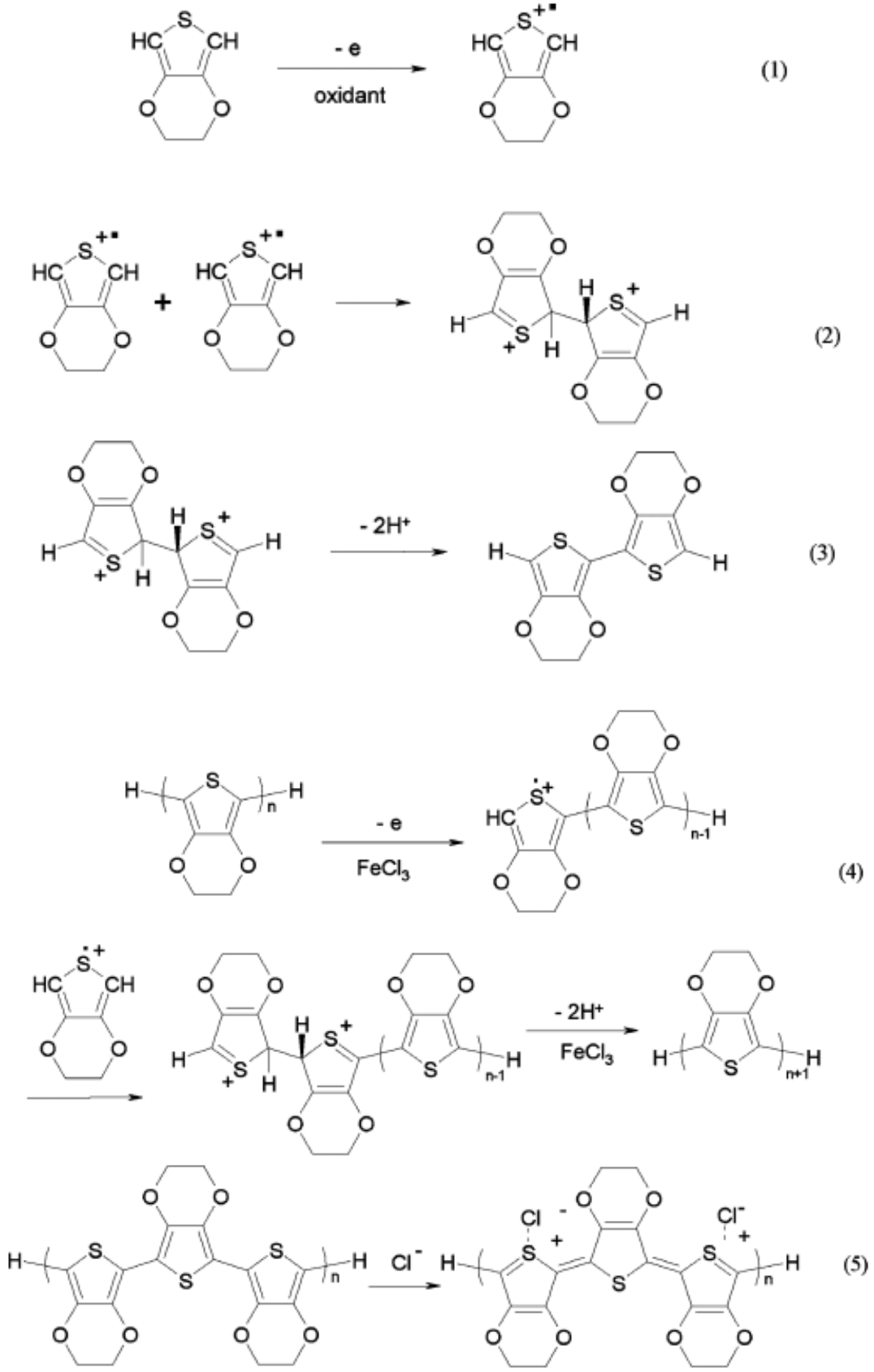

Figure 26. Five steps polymerization process of PEDOT: (1) Oxidation of EDOT to from cation radical; (2) Dimerization of cation radical; (3) Deprotonation to form conjugation; (4) Further

polymerization from n-mer to (n+1)-mer; (5) Doping process of PEDOT. Reference [45]

To briefly sum up all possible explanations up to now, the main factors that affect the conductivity of conducting polymers are shown below:

1. Polymer Chain (Length, shape)
2. Crystallinity
3. Counter-ion (additives that facilitate the polymer conductivity) and oxidized state
4. Temperature.

It is generally accepted that the conductivity of polymers obeys the following equation: [64]

$$\sigma = n \bullet \mu \bullet q$$

σ is the conductivity of the material, n is the number of carriers, q is the charge on the carriers and μ is the interchain and intrachain mobility of the carriers. The number of carriers and the charge on the carriers are determined by the oxidation state and courterion. The interchain and intrachain mobility of the carrier is influenced by chain length and crystallinity of conducting polymer.

3.4.1 Impact of Polymer Chain Length and Shape

The electronic band structure and the distribution of available electrons in the bands determine the electrical properties of the conducting polymer. [59] When the monomer

EDOT undergoes oxidization reaction during the polymerization process, the removal of electrons from the top of the valence band creates a vacancy, which is also called a hole or a radical cation. Instead of staying in the same position, the vacancy has partial delocalization over several monomeric units. The movement of vacancies creates polarons or bipolarons depending on the number of electrons lost on the site. [60] Both polarons and bipolarons are mobile and can move along the polymer chain by the rearrangement of double and single bonds in the conjugated system that occurs in an electric field. In addition to the movement of bipolarons (and polarons) in conducting polymers, the counterion must be taken into account in certain circumstances. But for electric measurements in the dry state, there is no movement of the counterions in the steady state since they are blocked at the electrodes. So these processes to some extent have close relationship with the polymerization process. [59] A preferred polymerization condition favors the longer polymer chain and it results in longer conjugation length. As the conducting mechanism of conducting polymer generally involves the transport of polaron and bipolaron along the polymer chain, the longer the conjugation length, the better the conductivity should be.

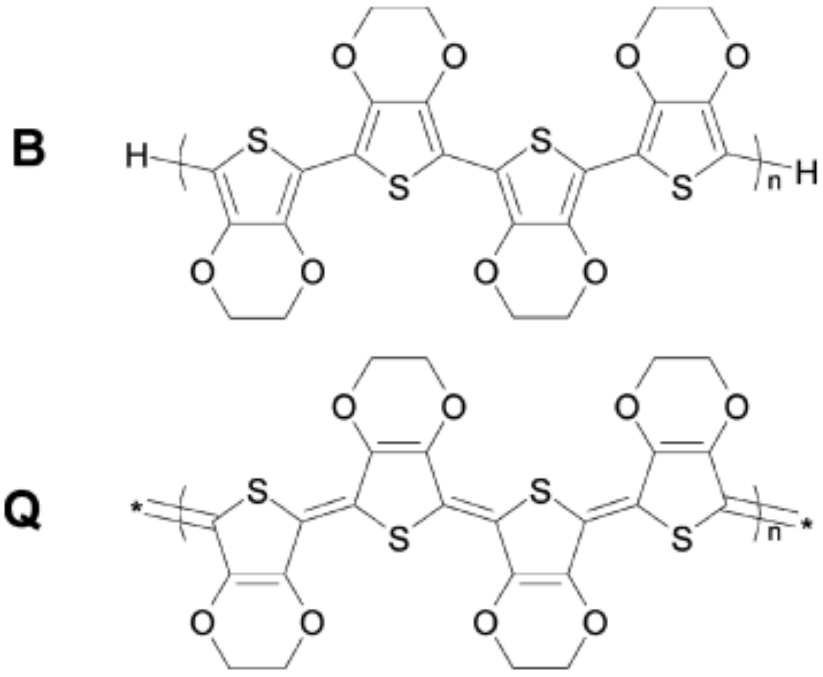

Figure 27. Benzoid (B) and quinoid (Q) types of PEDOT. Reference [45]

For PEDOT, there are two types of structures as is shown in figure 27: benzoid (B) and quinoid (Q). The benzoid structure may be the favorite structure for a coil conformation, while the quinoid structure may be the favorite structure for a linear or expanded-coil structure. [45] Therefore, it is proposed that both coil and linear or expanded-coil conformation turns into linear or expanded-coil conformation after the conductivity enhancement to some extent. It is understandable that the interaction among the PEDOT chains of linear conformation will be stronger than that among the PEDOT chain of coil conformation. [46] The structure difference can be identified with Raman spectroscopy as the symmetrical C_α=C_β stretching band (figure 28), which moved from around 1433 cm^{-1} to 1449 cm^{-1}, indicating that this vibration was sensitive to oxidizing (doping) and reducing (dedoping) behavior.

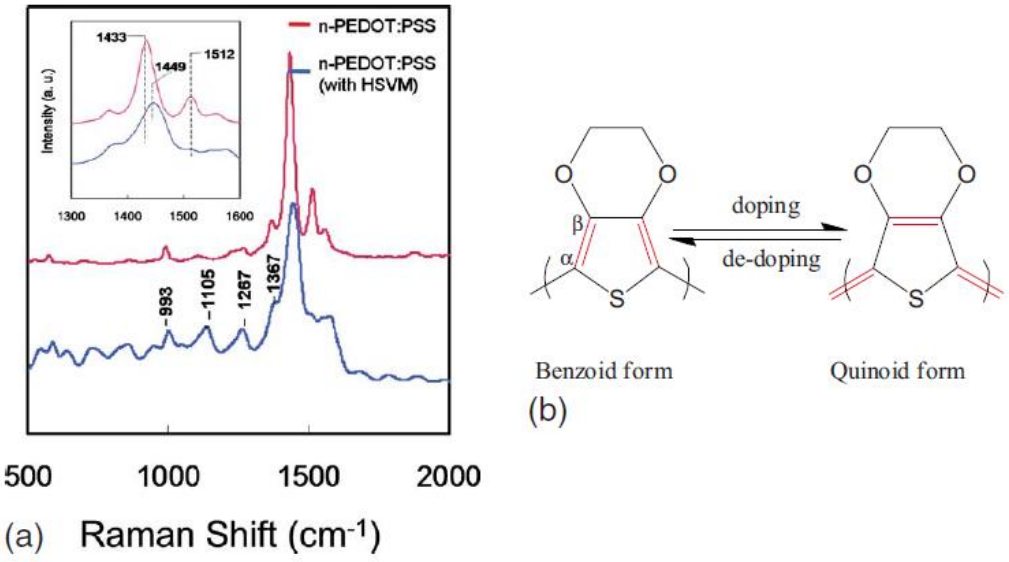

Figure 28. (a) Raman Spectra of n-PEDOT:PSS samples. (b) Benzoid and quinoid resonance strucutres. Reference [67]

Charge hopping among the polymer chains is believed to be the dominant conduction mechanism in almost all conducting polymers. [43] An increased interchain interaction should facilitate charge hopping among the conductive PEDOT chain. This point is addressed by the conductivity measurements of the PEDOT:PSS films from 295 K to liquid nitrogen temperature.

3.4.2 Impact of Crystallinity

In contrast to a semiconductor solid, such as silicon, the structure of a conjugated polymer is by far less regular. Polymers contain individual molecules with different chain length, varying amounts of defects, and chain ends; furthermore, they can be amorphous or

partially crystalline. Additional differences occur due to aging. Finally, the polymer chains can have orientation in x, y, and z direction resulting in different electronic properties. As a consequence, the disorder in conjugated polymers has a strong effect on the electronic properties. Generally speaking, disorder leads to the localization of charges.

However, order itself is not a sufficient condition for charge transport, since even in a highly ordered system, macroscopic charge transport is not possible unless the charges can hop or diffuse from one chain to another. Previous research reveals that increasing the crystallinity of conjugated polymers boosts the charge mobility and conductivity. Recently, several groups have published results showing disordered films with surprisingly high mobility and conductivity, which contradicts the idea that high carrier mobility is unambiguously linked to the degree of order of the materials. [61] Although the packing order in the novel, high-molecular-weight polymers is usually poor, the long and semirigid chains ensure domain interconnectivity, thus effectively increasing the charge mobility in these materials. [61]

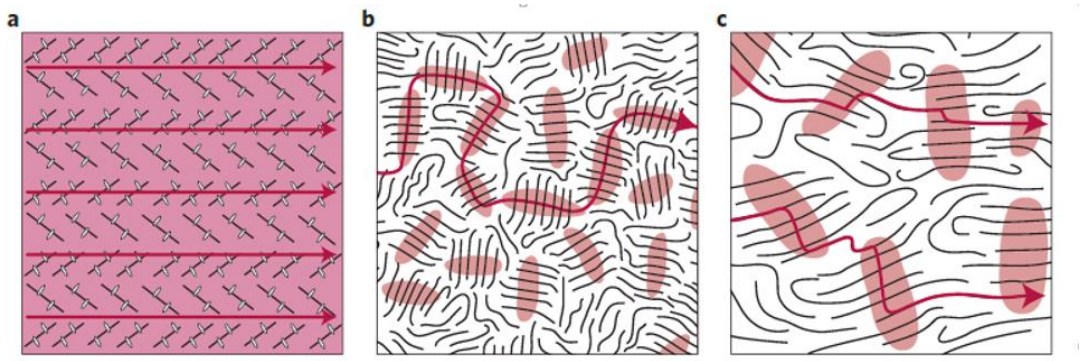

Figure 29 Order and charge transport in organic semiconductors. ***a****, Tight packing of molecules*

(black) in organic crystals may result in macroscopically long-range structural order and charge delocalization (red background). ***b****, The packing of small-to-medium molecular weight conjugated polymers can be sufficiently good on the nano- and microscale to form small ordered domains, but these domains are not well connected, resulting in transport bottlenecks at the grain boundaries.* ***c****, The packing order in the novel, high-molecular-weight polymers is usually poor, but the long and semirigid chains ensure domain inter connectivity, thus effectively increasing the charge mobility in these materials. The charge-motion paths are shown by the red arrows. The red shaded regions in* ***b*** *and* ***c*** *indicate charge delocalization occurring in ordered domains. Reference [61]*

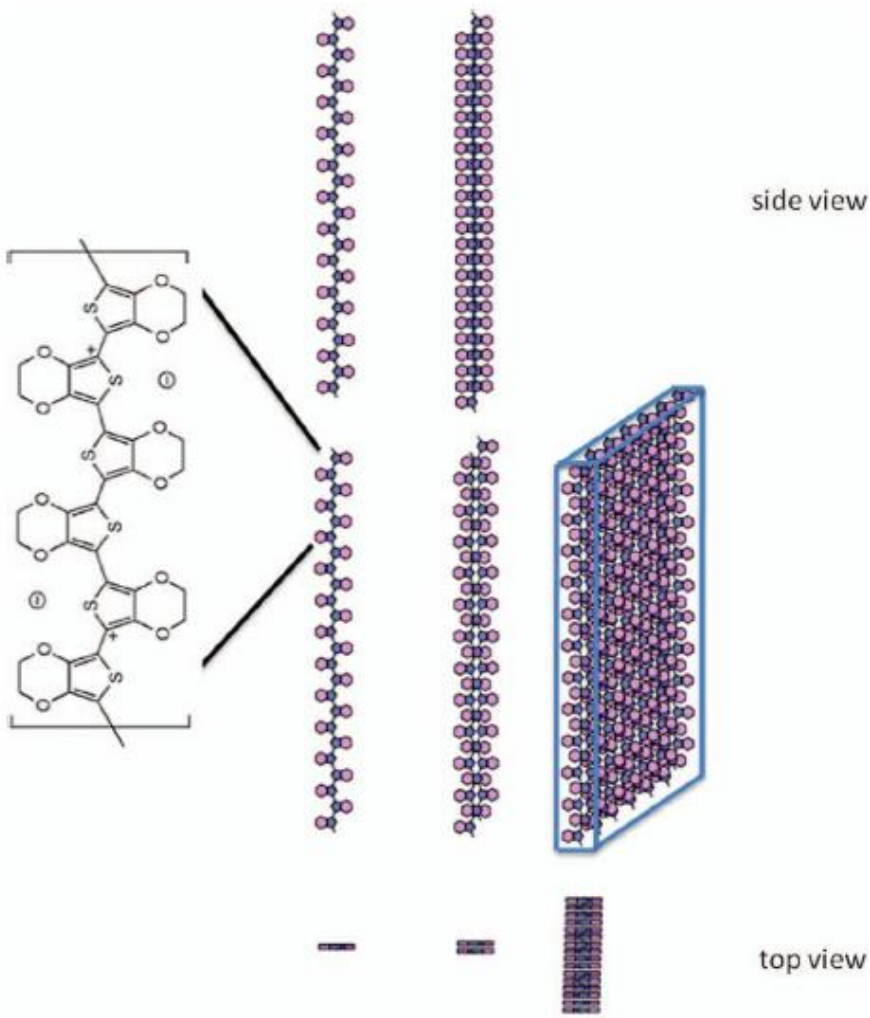

Figure 30. The geometry and assembly of single PEDOT chains into two chain PEDOT molecular complexes and then PEDOT sheets. Top: Side view ([010] projection), middle: oblique view, bottom: top view ([001] projection). Reference [3]

In the case of PEDOT:PSS, it can be described as a heterogeneously disordered conjugated polymer. The large disorder in PEDOT:PSS is a major difference to other conductive

polymers such as polyacetylene or polypyrrole. There is no crystalline structure observed in PEDOT:PSS film by x-ray analysis, but the existence of a lower degree of order has been shown that is not detected by x-ray analysis but does have a strong effect on the charge transport. Hence, models for disordered conjugated polymers are of particular interest to describe in PEDOT. New charge carriers can be introduced into conjugated polymers by the different types of doping described earlier. To participate in charge transport these charge carriers need to be mobile. For PEDOT the crystalline order is limited but by optimizing the synthesis method and condition, relatively high ordered PEDOT can still be achieved. Figure 30 illustratively shows how the PEDOT chains assemble into a PEDOT sheet and eventually form the PEDOT crystal structure. It has been reported that for the relatively high packing order of PEDOT has been synthesized via optimizing the deposition current density. Jinghang et al, changed the deposition current densities from 5 $\mu A/cm^2$ to 180 $\mu A/cm^2$. The deposition time is varied with the current densities as to make the same amount of charge passing through the substrate or form the same film thickness. The higher the deposition current densities, the higher the crystallinity. The center of the diffraction peaks are not influenced by varying different deposition current density. The crystallinity ranges from 20.5 wt % to 35 wt % as the current increased from 5 $\mu A/cm^2$ to 180 $\mu A/cm^2$. [3]

3.4.3 Impact of Counterion and Oxidized State of Polymer

The number of counterions needed for a certain length of PEDOT chain determines the

oxidation state of the polymer. [62] The number of carriers is determined by the doping level of the conducting polymer, which is controlled by the last step of polymerization. Additionally, the counterion can influence the spacing of PEDOT crystalline structure as is shown in figure 31. It is reasonable to assume that this affect is caused by the size and charge of the counterion. From table 6, we can find out that with the same charge, the bigger the anion, the larger the distance between each two crystal phase.

Actually those factors interact with each other and often appear to have comprehensive influence on the material's property. Higher temperature for surface polymerization will increase cation radical reactivity and accelerate dimerization and polymerization reactions because the reaction rate constants will increase with higher temperature. Thus, as reaction rate increase, monomer and oligomer cation radicals are more easily formed and then combine with each other to form stable high molecular weight chains until the high chain length lack the mobility limiting the mass transfer of radical cations. Chain mobility will also improve with increasing substrate temperature. This also promote deprotonation reaction to form conjugation due to increased reaction rate constant at higher temperature. Therefore, the extent of the deprotonation reaction is directly related to the length of conjugation. Then it follows that the conjugation length is governed by molecular weight of polymer and the degree of deprotonation of the polymer chain. Moreover, the scavenged protons are easily evaporated in the form of HCl. Since the back-bonded dioxyethelene ring can be possibly destroyed by acid-catalyzed reactions, the rapid elimination of HCl is desirable to prevent formation of defects along the chain. Thus, this promotes the formation of higher molecular weight chains and also decreases the density

of defects along the chain caused by insufficient deprotonation or unwanted acid-catalyzed side reactions. Therefore, the conjugation length will depend upon the completeness of each stepwise polymerization reaction.

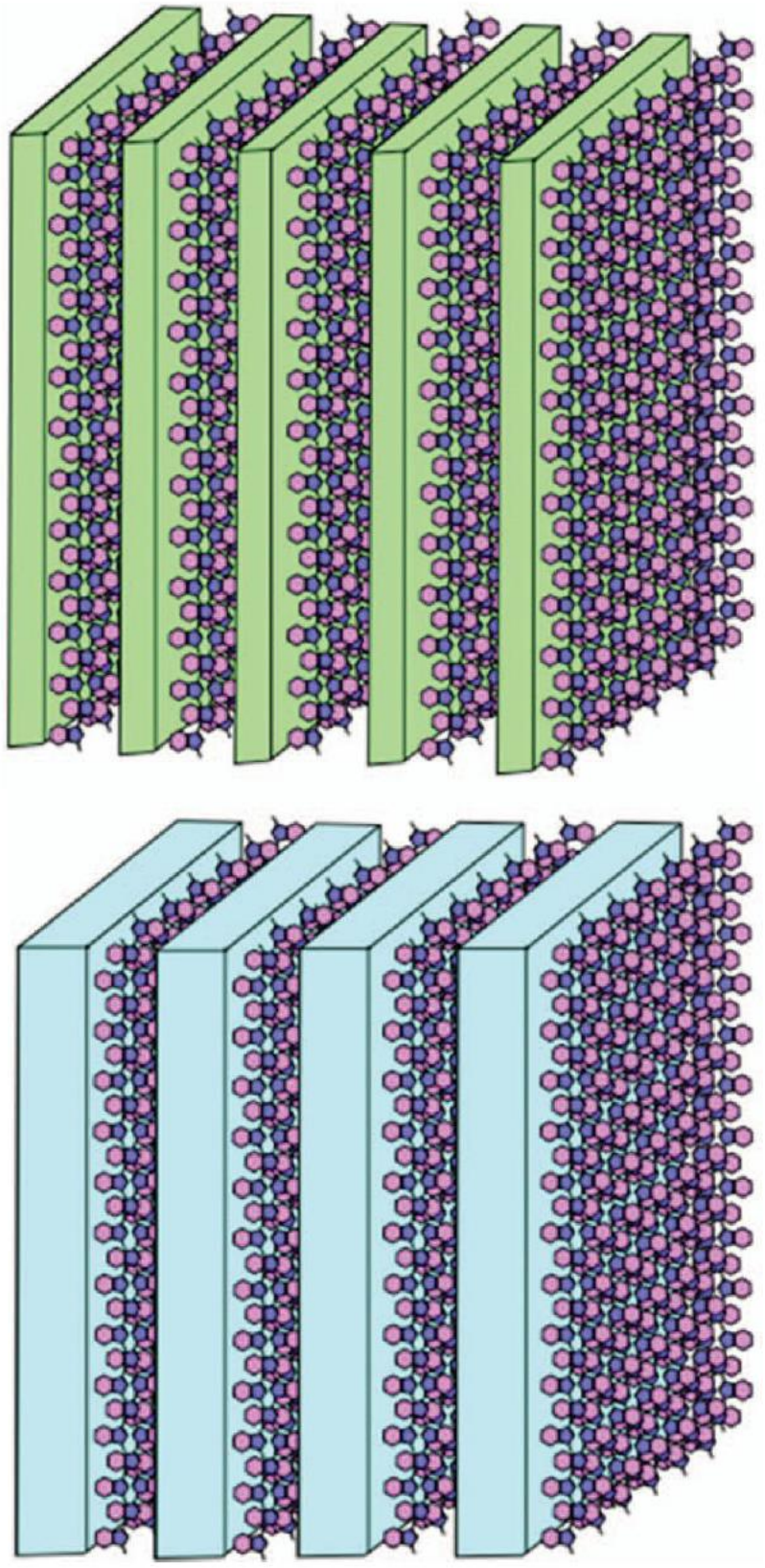

Figure 31. Schematic of the variation in microstructure of crystalline PEDOT with different dopants causing the (100) sheets of PEDOT chains to be closer together (green) or farther apart (blue) depending on the chemistry of the counterions used. Reference [3]

Table 6. (100) d-Spacing of PEDOT as a function of counterion chemistry. Reference [3]

(100) *d*-Spacings of PEDOT as a function of counterion chemistry

Counterion	d_{100} (nm)
PAA^-	1.52
PSS^-	1.46
PTS	1.39
Cl^- (NaCl)	1.39
$C_{14}SO_3$	1.37
Cl^- ($CaCl_2$)	1.33
EBS	1.32
CSA	1.29
F^-	1.15

3.5 Raman Spectroscopy Study of PEDOT Nanowire

Raman spectra of the series of PEDOT nanowires are shown in Figure 32 and Figure 33. The obtained Raman spectra are similar to one another and have the same primary features as that of PEDOT grown from other methods. The theoretical Raman shift calculations are shown in table 7. Several peaks of Raman shift below 800 cm^{-1} cannot be observed due to the Raman spectrum window we have chosen. Characteristic peaks of well-defined PEDOT, such as symmetric C_α=C_β symmetric stretching peak at around 1444 and 1428 cm^{-1} and C_β-C_β stretching peak at 1368 cm^{-1} are clearly observed.

Pan et al. assigned these peaks as undoped benzoidal vibration for the peak at 1428 cm^{-1} and doped quinoidal vibration for 1444 cm^{-1} in the PEDOT:PSS film. [67] Ouyang et al.

observed that the conductivity of PEDOT:PSS film was increased as the Raman peak was shifted from benzoid to doped quinoid. The Kelley group demonstrated these two structures by reducing as received PEDOT:PSS films. As we can see from figure 34, Raman spectra of as-received PEDOT:PSS film has two peaks around 1440 cm^{-1} at three different excitation wavelengths. When they reduced these films via hydrazine, the corresponding spectra became one single peak around 1440 cm^{-1} [65]. It is concluded that the totally reduced form of PEDOT only comprised benzoid structure while the as received PEDOT have both benzoid and quinoid structure. In figure 33, variation in the doping level was observed in the Raman spectrum. The peak at 1443 cm^{-1} and a shoulder of 1454 cm^{-1} are observed in figure 33, which indicates that both the quinoidal and benzoidal structures are present in the synthesized PEDOT nanowire. Compared to the PEDOT nanowires deposited under 50s and 80s, the shoulder to peak ratio of PEDOT nanowire synthesized under 120s is larger. Thus, the conductivity of PEDOT nanowire comprising of larger portion quinoidal structure is comparatively higher.

Table 7. Calculated Raman shift frequencies of PEDOT (Tran-Van, Garreau, Louarn, Froyer & Chevrot, 2001)

Calculated frequencies (cm^{-1})	
1509	C=C stretching in plane modes (antisym.)
1444	C==C stretching in plane modes (sym.)
1366	C-C stretching in plane modes
1267	C-C inter-ring stretching in plane modes

1228	C-C inter-ring stretching in plane modes
1061	C-O stretching
988	Oxyethylene ring deformation
865	O-C-C deformation
565	C-O-C deformation
440	C-O-C deformation

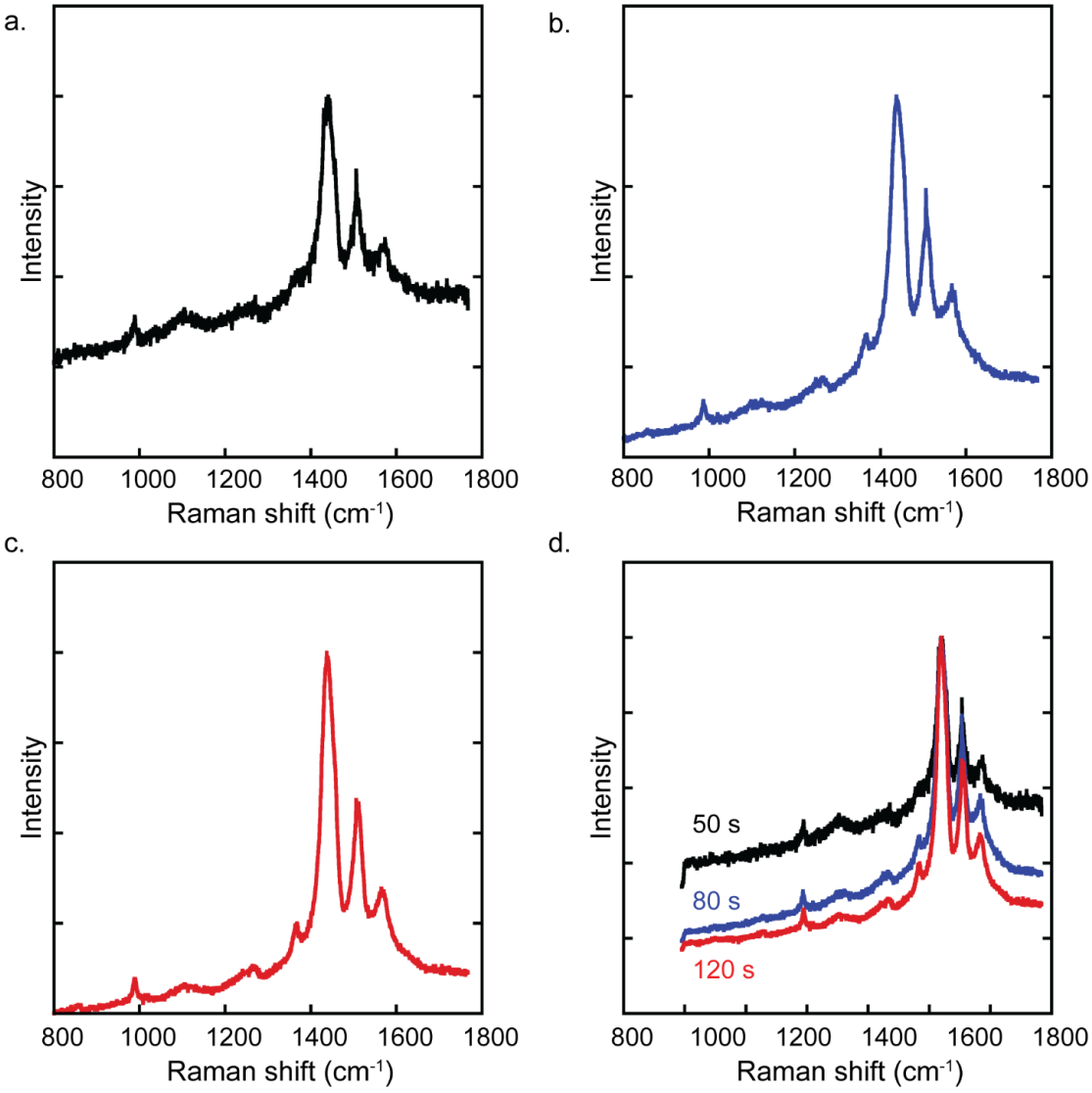

Figure 32. Raman spectrum of the synthesized PEDOT nanowires with the synthesis condition: deposition voltage 1.0 V and deposition time 50s, 80s, 120s respectively.

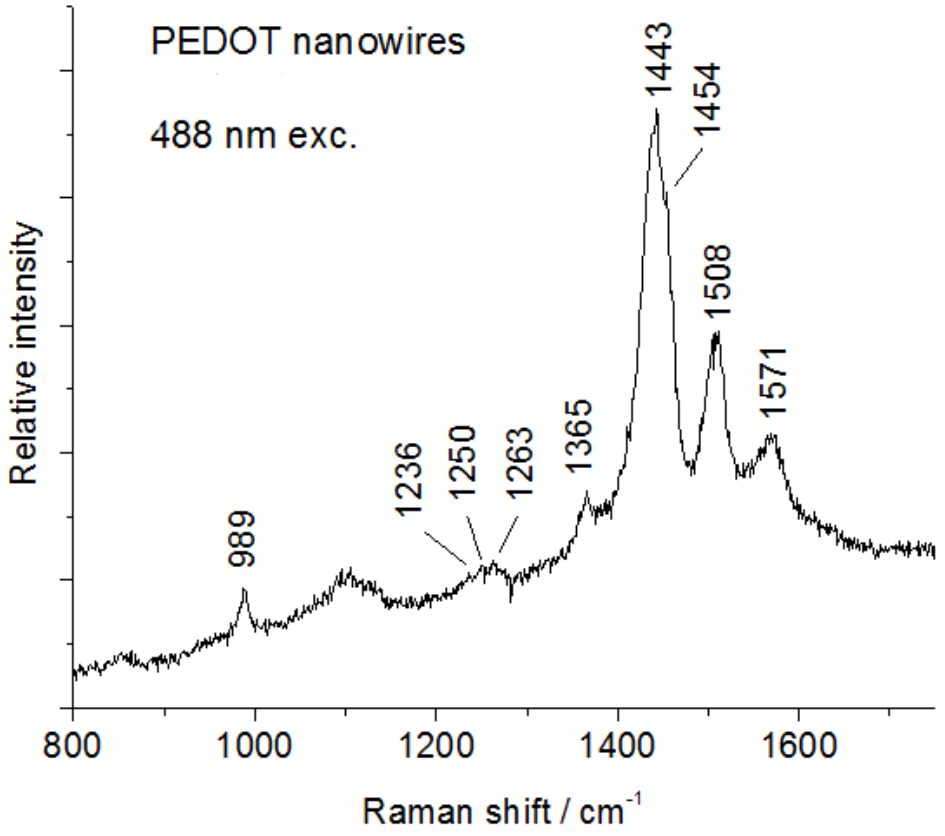

Figure 33. The graph is a sum of two nearly identical spectra taken on different parts of the same nanowire which was synthesized under 1.0 V and 120s.

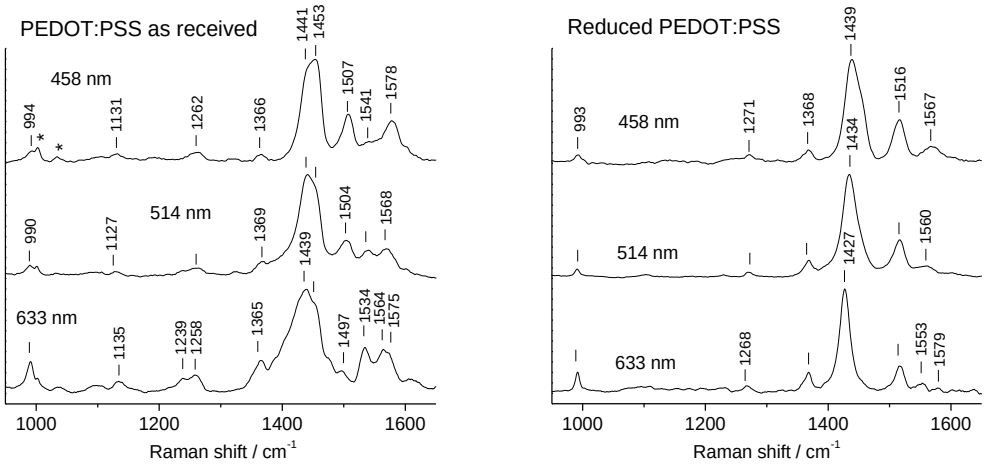

Figure 34. Left: Raman spectra of as-received PEDOT:PSS film at three excitation wavelengths. Right: Corresponding spectra of PEDOT:PSS film reduced with hydrazine. Reference [65]

3.6 Specific Capacitance of PEDOT Nanowires

In order to get the specific capacitance of the synthesized PEDOT nanowires, the mass and the capacitance of PEDOT nanowires are necessary to be obtained according to the equation which is listed below.

$$SC = \frac{C}{M}$$

SC: specific capacitance, C: capacitance, M: Mass.

We can get the capacitance of PEDOT nanowire from either cyclic voltammetry (CV) or electrochemical impedance spectroscopy (EIS). However, it's too noisy to do cyclic voltammetry study of PEDOT nanowires, especially those bare PEDOT nanowires without nickel contact. So we utilized EIS to determine the capacitance of PEDOT nanowires.

For capacitors, the imaginary component of the impedance $Z_{img} = 1/j\omega C$. Thus, we can get capacitance simply by plugging in this equation $C = 1/j\omega Z_{img}$ after we get the Z_{img} information from EIS. Here, Z represents the imaginary impedance, which you can read directly from the Y axis of the EIS graph. The set-up of the EIS measurement is basically very similar to the three-electrode electrochemical cell shown in figure 8 except the solution we are using is 1.0 M Na_2SO_4. The frequency range we are measuring is quite wide from as low as 0.1 Hz to a high of 100 kHz but in the application of capacitors, the properties in the high frequency range are what we care about. In the following calculations of five different samples, the data of 10 kHz to 100 kHz were averaged for each

sample in order to get the specific capacitance of the synthesized PEDOT nanowire. Also, from the polymerization process of PEDOT, we can elucidate the relationship between the charge transfer and the mass. As the oxidation polymerization process goes, three electrons were gradually lost among each three monomer of PEDOT and one more electron was lost due to the doping process if PEDOT is fully doped with counterion. [66]

$$\frac{Q}{4\ mol\ e} = \frac{M}{3 * 142.18\ g}$$

$$Q = \int Idt$$

$$C = \frac{1}{2 * pi * f * Zim}$$

$$SC = \frac{C}{M} = \frac{4\ mol * e}{2 * pi * f * Zim * Q * 3 * 142.18g} = 4\frac{Farad}{2 * pi * f * Zim * Q * 3 * 142.18g}$$

Deposition Curve and EIS for PEDOT nanowire under 40s deposition time are shown in figure 35 and 36 as an example. From this curve, we can calculate the charge by accumulating the area below the curve.

$$\mathrm{M} = \mathrm{Q} * 3 * \frac{142.18\mathrm{g}}{4\ mol * e} = Q * 3 * \frac{142.18g}{4\ Farads} = 0.000133 Coulomb * 3 * \frac{142.18g}{4\ Farads}$$
$$= Q(Coulomb) * \frac{1.107}{1000}\ g$$

a. PEDOT, 40s

Q_{40s}= 1.33*10^{-4} Coulomb.

M_{40s}=1.472*10^{-7} g.

$C = \frac{1}{5}\sum\frac{1}{2*pi*f*Zim}$ = 2.78*10 $^{-11}$ s/ohm=2.78*10^{-11} Farads

SC= C/M= $1.89*10^{-4}$ Farads/g

b. PEDOT, 60s

$M_{60s}=2.568*10^{-7}$ g.

$C = \frac{1}{5}\sum\frac{1}{2*pi*f*Zim}$ = $1.60*10^{-11}$ s/ohm=$1.60*10^{-11}$ Farads

SC= C/M= $6.23*10^{-5}$ Farads/g

c. PEDOT, 80s

$M_{60s}=4.455*10^{-7}$ g.

$C = \frac{1}{5}\sum\frac{1}{2*pi*f*Zim}$ = $1.75*10^{-11}$ s/ohm=$1.75*10^{-11}$ Farads

SC= C/M= $3.93*10^{-5}$ Farads/g

d. PEDOT, 100s

$M_{60s}=1.560*10^{-7}$ g.

$C = \frac{1}{5}\sum\frac{1}{2*pi*f*Zim}$ = $3.25*10^{-10}$ s/ohm=$3.25*10^{-10}$ Farads

SC= C/M= $2.08*10^{-3}$ Farads/g

e. PEDOT, 120s

$M_{120s}=3.605*10^{-7}$ g.

$C = \frac{1}{5}\sum\frac{1}{2*pi*f*Zim}$ = $9.69*10^{-9}$ s/ohm=$9.69*10^{-9}$ Farads

SC= C/M= 2.69 *10^{-2} Farads/g

f. PEDOT, 140s

M_{120s}=3.670 *10^{-7} g.

$C = \frac{1}{5}\sum \frac{1}{2*pi*f*Zim}$ = 1.04*10 $^{-8}$ s/ohm=1.04*10^{-8} Farads

SC= C/M= 2.83*10^{-2} Farads/g

From table 8, we can clearly see that PEDOT nanowires under the deposition time exceeding 100 seconds have a much larger specific capacitance than those nanowires under 100s deposition time. When we compare these values with the commercially available capacitors (tantalum powder capacitor, 30000 μC/g), it turns out that the synthesized PEDOT nanowires have much bigger specific capacitance as the tantalum powder capacitor only has about 3.1×10^{-7} Farads/g. Also, they possessed higher specific capacitance than the reported conducting polymer dispersion, which is 15 μFarads/g. [66]

Table 8. A summary of the specific capacitance of PEDOT nanowires under different deposition time

Deposition Time (s)	Specific Capacitance (Farads/g)
40	1.89*10^{-4}
60	6.23*10^{-5}
80	3.93*10^{-5}
100	2.08*10^{-3}
120	2.69*10^{-2}
140	2.83*10^{-2}

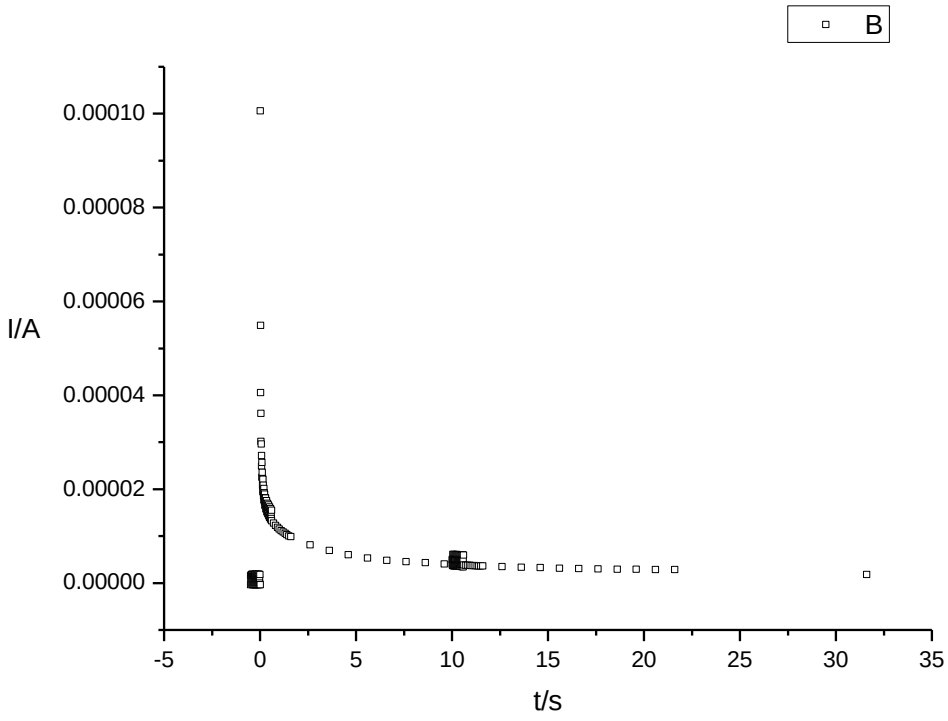

Figure 35. Chronoamperometry deposition curve of PEDOT nanowire in 40s

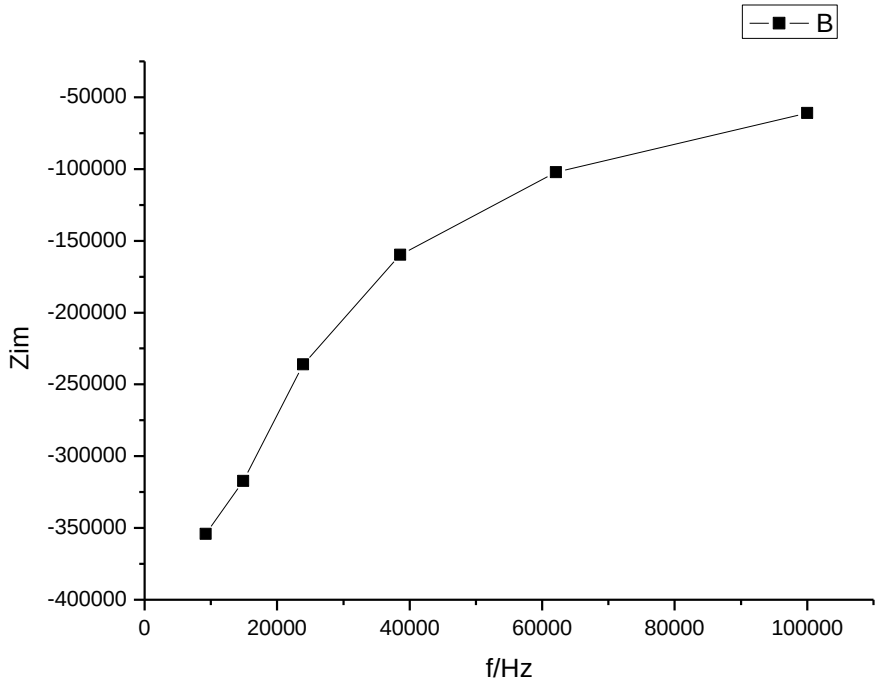

Figure 36. Electrochemical Impedance Spectrum of PEDOT nanowire from 10 kHz to 100 kHz under the deposition time of 40s.

4. Conclusion

The electrochemical polymerization of 3,4-ethylenedioxythiophene (EDOT) in lithium perchlorate electrolyte aqueous solution was studied in order to establish a direct relationship between the synthesis conditions and the properties of PEDOT nanowires. By applying the feasible lithographically patterned nanowire electrodeposition method (LPNE), PEDOT nanowires of different size and morphology were successfully synthesized. Optical microscope, AFM measurements show the various electrodeposition parameters (deposition methods, deposition voltage, deposition time, template size, etc.) have a great impact on the materials properties of the prepared nanowires.

By comparing the resulting nanowires, we have been able to determine the optimal synthesis condition for PEDOT nanowire. Under chronoamperometry, we observed a nearly linear relationship between the deposition time and the width of PEDOT nanowires. The height dimension confinement makes the polymerization kinetics different from the observed 3D polymerization model, which explains the nearly linear growth. Raman spectroscopy further demonstrate the quinoidal structure is key to the conductivity enhancement of PEDOT nanowire. We also calculated the capacitance from EIS measurement and mass from the polymerization curve of PEDOT. The specific capacitance of each PEDOT nanowire is calculated in order to compare with the commercially available capacitors. It turns out that once the deposition time exceeds 100 seconds, the specific

capacitance is becoming more than ten times larger than those nanowires under 100s deposition time.

The synthesized PEDOT nanowires exhibit superior specific capacitance when compared to the commercially available capacitors and even conducting polymer dispersion based capacitors. The reason we suspect is that the confinement of height afford an optimized polymerization of PEDOT besides the fine morphology and large surface area of the nanowires. However, this observed phenomenon is more interesting than that and it definitely requires further experiments to make it clear.

Reference

1. Jianyong Ouyang, Chi-Wei Chu, Fang-Chung Chen, Qianfei Xu and Yang Yang, "High-conductivity poly(3,4-ethylenedioxythiophene):poly(styrenesulfonate) film and its application in polymer optoelectronic devices", Adv. Funct. Mater., 2005, February, 15, No. 2

2. Jurgen Heinze, Bernardo A. Frontana-Uribe, and Sabin Ludwigs, "Electrochemistry of conducting polymers-persistant models and new concepts", Chem. Rev, 2010, Vol, 110, No. 8

3. Jinghang Wu, "Morphology of poly(3,4-ethylenedioxythiophene) thin films, crystals, cubic phases, fibers and tubes", Thesis, University of Michigan, 2011

4. Henry D. Tran, Dan Li, and Richard B. Kaner, "One-Dimensional conducting polymer nanostructures bulk synthesis and applications", Adv. Mater. 2009, 21, 1487-1499

5. L. "Bert" Groenendaal, Friedrich Jonas, Dieter Freitag, Harald Pielartzik, and John R. Reynolds, "Poly(3,4-ethylenedioxythiophene) and its derivatives: past, present, and future" Adv. Mater, 2000, 12, No. 7

6. Dasaroyong Kim, Yeonseok Kim, Kyungwho Choi, Jaime C. Grunlan, and Choongho Yu, "Improved thermoelectric behavior of nanotube-filled polymer composites with poly(3,4-ethylenedioxythiophene):poly(styrenesulfonate)", ACS Nano., Vol 4, No. 1, 2010, 513-523

7. B. Zhang, J. Sun, H. E. Katz, F. Fang, and R. L. Opila, "Promising thermoelectric properties of commercial PEDOT:PSS materials and their Bi_2Te_3 powder composites", Applied Materials & Interfaces, Vol. 2, No. 11, 2010, 3170-3178

8. Byeonggwan Kim, Haijin Shin, Teahoon Park, Hanwhuy Lim, and Eunkyoung Kim, "NI-Sensitive poly(3,4-ethylenedioxyselenophene) derivatives for transparent photo-thermo-electric converters", Adv. Mater. 2013, 25, 5483-5489

9. Mario Leclerc and Ahmed Najari, "Green energy from a blue polymer", Nature Materials, Vol 10, June 2011, 409-410

10. Roland Steim, F. Rene Kogler and Christoph J. Brabec, "Interface materials for organic solar cells", J. Mater. Chem., 2010, 20, 2499-2512

11. Robert F. Service, "Outlook brightens for plastic solar cells", Science, 2011, April 15, Vol 332, 293

12. Joung Eun Yoo, Kwang Seok Lee, Andres Garcia, Jacob Tarver, Enrique D. Gomez, Kimberly Baldwin, "Directly patternable, highly conducting polymers for broad applications in organic electronics", 5712-5717, PNAS, March 30, 2010, Vol 107, No. 13

13. Daniel E. Lopez-Perez, David Aradilla, Luis J. del Valle, and Carlos Aleman, "Capacitive composites made of conducting polymer and lysozyme toward the biocondenser", J. Phys. Chem. C 2013, 117, 6607-6619

14. Yijie Xia, Jianyong Ouyang, "Anion effect on salt-induced conductivity enhancement of poly(3,4-ethylenedioxythiophene):poly(styrenesulfonate) films", Organic Electronics 11, 2010, 1129-1135

15. Jianyong Ouyang, Qianfei Xu, Chi-Wei Chu, Yang Yang, Gang Li, Joseph Shinar, "On the mechanism of conductivity enhancement in poly(3,4-ethylenedioxythiophene): poly(styrene sulfonate) film through solvent treatment", Polymer 45, 2004, 8443-8450

16. O. P. Dimitriev, D.A. Grinko, Yu. V. Noskov, N. A. Ogurtsov, A. A. Pud, "PEDOT:PSS

films-effect of organic solvent additives and annealing on the film conductivity", Synthetic Metals 159, 2009, 2237-2239

17. Leif Nyholm, Gustav Nystrom, Albert Mihranyan, and Maria Stromme, "Toward flexible polymer and paper-based energy storage devices", Adv. Mater. 2011, 23, 3751-3769

18. Michael G. Helander, "Solution-processible electrodes", Science 336, 302, 2012

19 Lizhi Zhan, Zhiping Song, Jingyu Zhang, Jing Tang, Hui Zhan, Yunhong Zhou, Caimao Zhan, "PEDOT: Cathode active material with high specific capacity in novel electrolyte system", Electrochimica Acta 53 (2008) 8319-8323

20. A. Zykwinska, W. Domagala, M. Lapkowski, "ESR spectroelectrochemistry of poly(3,4-ethylenedioxythiophene) (PEDOT)", Electrochemistry Communication 5 (2003) 603-608

21. Xinyan Cui, David C. Martin, "Electrochemical deposition and characterization of poly(3,4-ethylenedioxythiophene) on neural microelectrode arrays", Sensors and Actuators B 89 (2003) 92-102

22. Kip A Ludwig, Jeffrey D Uram, Junyan Yang, David C Martin and Daryl R Kipke, "Chronic neural recordings using silicon microelectrode arrays electrochemically deposited with a poly(3,4-ethylenedioxythiophene) (PEDOT) film", J. Neural Eng. 3 (2006) 59-70

23. Punya A. Basnayaka, Manoj K. Ram, Lee Stefanakos and Ashok Kumar, 'Poly (acrylic acid) - mediated soft template synthesis of Poly (3, 4-ethylenedioxythiophene)-based conducting polymer nanostructures for supercapacitor applications", Mater. Res. Soc. Symp. Proc. Vol. 1497

24. Yu Li, Bichen Wang, Huimin Chen, Wei Feng, "Improvement of the electrochemical properties via poly(3,4-ethylenedioxythiophene) oriented micro/nanorods", Journal of Power Sources 195 (2010) 3025-3030

25. Julio M. D'Arcy, Maher F. El-Kady, Pwint P. Khine, Linghong Zhang, Sun Hwa Lee, Nicole R. Davis, David S. Liu, Michael T. Yeung, Sung Yeol Kim, Christopher L. Turner, Andrew T. Lech, Paula T. Hammond, and Richard B. Kaner, "Vapor-phase polymerization of nanofibrillar poly(3,4-ethylenedioxythiophene) for supercapacitors", ACS Nano, 2014, 8 (2), pp 1500–1510

26. Ran Liu, Seung Il Cho and Sang Bok Lee, "Poly(3,4-ethylenedioxythiophene) nanotubes as electrode materials for a high-powered supercapacitor", Nanotechnology 19 (2008) 215710 (8pp)

27. Qiang Zhang, Fei Wei, "Advanced Hierarchical Nanostructured Materials", John Wiley & Sons, Feb 14, 2014

28. S. I. Cho, S.B. Lee, 'Fast electrochemistry of conductive polymer nanotubes: synthesis, mechanism, and application", Acc Chem Res. 2008, 41, 699.

29. Marc Lepeltier, Jonathan Hiltz, Tobias Lockwood, Francine Belanger-Gariepy and Dmitrii F. Perepichka, "Towards crystal engineering of solid-state polymerization in dibromothiophenes", J. Mater. Chem., 2009, 19, 5167-5174

30. Wanli Ma, Parameswar K. Iyer, Xiong Gong, Bin Liu, Daniel Moses, Guillermo C. Bazan, and Alan J. Heeger, "Water/Methanol-Soluble Conjugated Copolymer as an Electron-Transport Layer in Polymer Light-Emitting Diodes ", Adv. Mater. 2005, 17, No. 3, February 10

31. Seok-In Na, Seok-Soon Kim, Jang Jo, and Dong-Yu Kim, "Efficient and Flexible ITO-Free Organic Solar Cells Using Highly Conductive Polymer Anodes", Adv. Mater. 2008, 20, 4061-4067

32. Wen Lu, Andrei G. Fadeev1, Baohua Qi, Elisabeth Smela, Benjamin R. Mattes, Jie Ding, Geoffrey M. Spinks, Jakub Mazurkiewicz, Dezhi Zhou, Gordon G. Wallace, Douglas R. MacFarlane, Stewart A. Forsyth, Maria Forsyth. "Use of Ionic Liquids for π-Conjugated Polymer Electrochemical Devices", Science 297, 983 (2002)

33. L. Groenendaal, G. Zotti, F. Jonas, "Optical, conductive and magnetic properties of electrochemically prepared alkylated poly(3,4-ethylenedioxythiophene)s", Synthetic Metals 118 (2001) 105-109

34. L. "Bert" Groenendaal, Friedrich Jonas, Dieter Freitag, Harald Pielartzik, and John R. Reynolds, "Poly(3,4-ethylenedioxythiophene) and its derivatives: past, present, and future", Adv. Mater. 2000, 12, No.7

35. Bjorn Winther-Jensen, Orawan Winther-Jensen, Maria Forsyth, Douglas R. Macfarlane, "High rates of oxygen reduction over a vapor phase–polymerized PEDOT electrode", Science 321, 671 (2008)

36. Micheal Vosgueritchian, Darren J. Lipomi, and Zhenan Bao, 'Highly conductive and transparent PEDOT:PSS films with a fluorosurfactant for stretchable and flexible transparent electrodes', Adv. Funct. Mater. 2012, 22, 421-428

37. Bjorn Winther-Jensen, Frederik C. Krebs, "High-conductivity large-area semi-transparent electrodes for polymer photovoltaics by silk screen printing and vapour-phase deposition", Solar Energy Materials & Solar Cells 90 (2006) 123-132

38. J. Huang, P.F. Miller, J.C. de Mello, A.J. de Mello, D.D.C. Bradley, "Influence of thermal treatment on the conductivity and morphology of PEDOT/PSS films", Synthetic Metals 139 (2003) 569-572

39. Alan G. MacDiarmid, ""Synthetic Metals": A Novel Role for Organic Polymers", Angew. Chem. Int. Ed. 2001, 40, 2581-2590

40. Kai Wang, Haiping Wu, Yuena Meng, and Zhixiang Wei, "Conducting polymer nanowire arrays for high performance supercapacitors", Small, 2014, 10, No. 1, 14-31

41. Zhigang Yin and Qingdong Zheng, "Controlled synthesis and energy applications of one-dimensional conducting polymer nanostructures: an overview", Adv. Energy Mater, 2012, 2, 179-218

42. Elena Poverenov, Mao Li, Arkady Bitler, and Michael Bendikov, "Major effect of electropolymerization solvent on morphology and electrochromic properties of PEDOT films", Chem. Mater. 2010, 22, 4019-4025

43. S. Garreau, J.L. Duvail, G. Louarn, "spectroelectrochemical studies of poly(3,4-ethylenedioxythiophene) in aqueous medium", Synthetic metals 125 (2002) 325-329

44. David K. Taggart, Yonggan Yang, Sheng-Chin Kung, Theresa M. McIntire, and Reginald M. Penner, "Enhanced thermoelectric metrics in ultra-long electrodeposited PEDOT nanowires", Nano Lett. 2011, 11, 125-131

45. Sung Gap Im and Karen K. Gleason, "Systematic control of the electrical conductivity of poly(3,4-ethylenedioxythiophene) via oxidative chemical vapor deposition", Macromolecules 2007, 40, 6552-6556

46. Jianyong Ouyang, Qianfei Xu, Chi-Wei Chu, Yang Yang, Gang Li, Joseph Shinarr, "On

the mechanism of conductivity enhancement in poly(3,4-ethylenedioxythiophene): poly(styrene sulfonate) film through solvent treatmen", Polymer 45 (2004) 8443-8450

47. E. J. Menke, M. A. Thompson, C. Xiang, L. C. Yang and R. M. Penner, "Lithographically patterned nanowire electrodeposition", Nature Materials, Vol 5, November 2006

48. Justin E. Hujdic, Alan P. Sargisian, Jingru Shao, Tao Ye and Erik J. Menke, "High-density gold nanowire arrays by lithographically patterned nanowire electrodeposition", Nanoscale, 2011, 3, 2697

49. Somnath Ghosh, Justin E. Hujdic, Alfredo Villicana-Bedolla, and Erik J. Menke, "Gold–semiconductor core-Shell nanowires prepared by lithographically patterned nanowire electrodeposition", J. Phys. Chem. C 2011, 115, 17670-17675

50. Emanuela Tamburri, Silvia Orlanducci, Francesco Toschi, Maria Letizia Terranova, Daniele Passeri, "Growth mechanisms, morphology, and electroactivity of PEDOT layers produced by electrochemical routes in aqueous medium", Synthetic Metals 159, 2009, 406-414

51. H. Randriamahazaka, V. Noel, C. Chevrot, "Nucleation and growth of poly(3,4-ethylenedioxythiophene) in acetonitrile on platinum under potentiostatic conditions", Journal of Electroanalytical Chemistry 472 (1999) 103-111

52. Winther-Jensen, B.; West, K., "Vapor-phase polymerization of 3,4-ethylenedioxythiophene: a route to highly conducting polymer surface layers", Macromolecules, 2004, 37, 4538-4543

53. Meng, H.; Perepichka, D. F.; Bendikov, M.; Wudl, F.; Pan, G. Z.; Yu, W. J.; Brown, S., "Solid-state synthesis of a conducting polythiophene via an unprecedented heterocyclic coupling reaction", J. Am. Chem. Soc. 2003, 125, 15151-15162

54. Bret D. Martin, Michael A. Markowitz, Brian Melde, "Mesoporous monoliths containing conducting polymers", US 20110223331 A1

55. S. Murali, S. Prasertpalichat, C. C. Huang, D. Cann, R. yimnirun, and J. F. Conley, Jr., "Conductivity measurement of ZnO nanowires using the powder-solution-composite technique", Journal of the Electrochemical Society, 158 (10) G211-G216, 2011

56. Yunze Long, Zhaojia Chen, Wenlong Wang, Fenglian Bai, Aizi Jin, and Changzhi Gu,

"Electrical conductivity of single CdS nanowire synthesized by aqueous chemical growth", Applied Physics Letters, 86, 153102, 2005

57. J Aguilar-Hernandez and K Potje-Kamloth, "Evaluation of the electrical conductivity of polypyrrole polymer composites", Appl. Phys. 34 (2001), 1700-1711

58. R. H. Baughman and L. W. Shacklette, "Conjugation length dependent transport in conducting polymers from a resistor network model", J. Chem, Phys. 90 (12), 15 June 1989

59. W. R. Salaneck, R. H. Friend, J. L. Bredas, "Electronic structure of conjugated polymers: consequences of electron-lattice coupling", Physics Reports, 319, (1999), 231-251

60. Kerileng M. Molapo, Peter M. Ndangili, Rachel F. Ajayi, Gcineka Mbambisa, Stephen M. Mailu, Njagi Njomo, Milua Masikini, Priscilla Baker and Emmanuel I. Iwuoha, "Electronics of conjugated polymers (I): polyaniline", Int. J. Electrochem. Sci., 7, 2012, 11859-11875

61. Rodrigo Noriega, Jonathan Rivnay, Koen Vandewal, Felix P. V.Koch, Natalie Stingelin, Paul Smith, Michael F. Toney and Alberto Salleo, "A general relationship between disorder, aggregation and charge transport in conjugated polymer", Nature Materials, VOL 12, Nov 2013

62. H. Randriamahazaka, V. Noel, C. Chevrot, "Nucleation and growth of poly(3,4-ethylenedioxythiophene) in acetonitrile on platinum under potentiostatic conditions", Journal of Electroanalytical Chemistry, 472 (1999) 103-111

63. Ailton De Souza Gomes, "New polymers for special applications", ISBN 978-953-51-0744-6, 366 pages, Publisher: InTech

64. Bube, Richard H. "Electrons in solids: An introduction survey" 3rd Edition, California, Academic Press Inc. 1992

65. Marina Stavytska-Barba and Anne Myers Kelley, "Surface-enhanced Raman study of the interface of PEDOT:PSS with plasmonically active nanoparticles", J. Phys. Chem. C 2010, 114, 6822-6830

66. Andreas Elschner, "PEDOT: principles and applications of an intrinsically conductive polymer", CRC Press, 2011.

67. Yukai Han, Meiying Chang, Wenyao Huang, Hsinyu Pan, koshan Ho, Tarhwa Hsieh, and Sinyu Pan, “Improved performance of polymer solar cells featuring one-dimensional PEDOT nanorods in a modified buffer layer”, J. Electrochem. Soc., 158 (3) K88-K93 (2011)